Evaluation of lipid biomarkers as proxies for sea ice and ocean temperatures along the Antarctic continental margin

Nele Lamping[1], Juliane Müller[1,2,3], Jens Hefter[1], Gesine Mollenhauer[1,2,3], Christian Haas[1], Xiaoxu Shi[1], Maria-Elena Vorrath[1], Gerrit Lohmann[1,3,4], Claus-Dieter Hillenbrand[5]

[1]Alfred Wegener Institute, Helmholtz Center for Polar and Marine Research, Am Alten Hafen 26, 27568 Bremerhaven, Germany

[2]Department of Geosciences, University of Bremen, Klagenfurter Straße, 28359 Bremen, Germany

[3]Marum - Center for Marine Environmental Sciences, Leobener Straße 8, 28359 Bremen, Germany

[4]Department of Environmental Physics, University of Bremen, 28359 Bremen, Germany

[5]British Antarctic Survey, High Cross, Madingley Road, Cambridge CB3 0ET, United Kingdom

Correspondence to: Nele Lamping (nele.lamping@awi.de)

Abstract

The importance of Antarctic sea ice and Southern Ocean warming has come into the focus of polar research in the last couple of decades. Especially in West Antarctica, where warm water masses approach the continent and where sea ice has declined, the distribution and evolution of sea ice play a critical role for the stability of nearby ice shelves. Organic geochemical analyses of marine seafloor surface sediments from the Antarctic continental margin permit an evaluation of the applicability of biomarker-based sea ice and ocean temperature reconstructions in these vulnerable areas. We analysed highly branched isoprenoids (HBIs), such as the sea-ice proxy $IPSO_{25}$ and phytoplankton-derived HBI-trienes, but also phytosterols and isoprenoidal glycerol dialkyl glycerol tetraethers (GDGTs), which are established tools for the assessment of primary productivity and ocean temperatures, respectively. The combination of $IPSO_{25}$ with a phytoplankton marker (*i.e.* the $PIPSO_{25}$ index) permits semi-quantitative sea ice reconstructions and avoids misleading over- or underestimations of sea-ice cover. Comparisons

of the $PIPSO_{25}$-based sea-ice distribution patterns and TEX^{L}_{86}- and RI-OH'-derived ocean temperatures with (1) sea-ice concentrations obtained from satellite observations and (2) instrumental sea surface and subsurface temperatures corroborate the general capability of these proxies to properly display oceanic key variables. This is further supported by model data. We also highlight specific aspects and limitations that need to be considered when interpreting such biomarker data and discuss the potential of $IPSO_{25}$ to reflect the former occurrence of platelet ice and/or the export of ice shelf water.

1. Introduction

One of the key components of the global climate system, influencing major atmospheric and oceanic processes, is floating on the ocean's surface at high latitudes – sea ice (Thomas, 2017). Southern Ocean sea ice is one of the most strongly changing features of the Earth's surface as it experiences considerable seasonal variabilities with decreasing sea-ice extent from a maximum of 20 x 10^6 km^2 in September to a minimum of 4 x 10^6 km^2 in March (Arrigo et al., 1997; Zwally, 1983). This seasonal waxing and waning of sea ice substantially modifies deep-water formation as well as the ocean-atmosphere exchange of heat and gas, strongly affects surface albedo and radiation budgets (Abernathey et al., 2016; Nicholls et al., 2009; Turner et al., 2017), and also regulates ocean buoyancy flux, upwelling and primary production (Schofield et al., 2018).

Based on the 40-year satellite record, Southern Ocean sea-ice extent as a whole followed an increasing trend (Comiso et al., 2017; Parkinson and Cavalieri, 2012), experiencing an abrupt reversal from 2014 to 2018 (Parkinson, 2019; Turner et al., 2020; Wang et al., 2019), which has been attributed to a decades-long oceanic warming and increased advection of atmospheric heat (Eayrs et al., 2021). In particular, the sea-ice extent around major parts of West Antarctica has been decreasing (Parkinson and Cavalieri, 2012), with the Antarctic Peninsula being affected by a significant reduction in sea-ice extent and rapid atmospheric and oceanic warming (Etourneau et al., 2019; Li et al., 2014; Massom et al., 2018; Vaughan et al., 2003). The Larsen Ice Shelves A and B, located east of the Antarctic Peninsula, collapsed in 1995 and 2002, respectively, which was triggered by the loss of a sea-ice buffer, enabling an increased flexure of the ice shelf margins by ocean swells (Massom et al., 2018). The Bellingshausen and Amundsen Seas are also affected by a major sea-ice decline and regional surface ocean warming (Hobbs et al., 2016; Parkinson, 2019). Marine-terminating glaciers draining into the Amundsen Sea are thinning at an alarming rate, which has been linked to sub-ice shelf melting caused by relatively warm Circumpolar Deep Water (CDW) incursions into sub-ice shelf cavities (*e.g.*, Jacobs et al., 2011; Khazendar et al., 2016; Nakayama et al., 2018; Rignot et al., 2019; Smith et al., 2017). The disintegration of ice shelves reduces the buttressing effect that they exert on ice grounded further upstream, which may lead to a partial collapse of the catchments of the affected glaciers, eventually

raising global sea level considerably (3.4 to 4.4 m resulting from a WAIS collapse; Fretwell et al., 2013; Jenkins et al., 2018; Pritchard et al., 2012; Vaughan, 2008).

State-of-the-art climate models are not yet fully able to depict sea-ice seasonality and sea-ice cover, which the 5th Assessment Report of the Intergovernmental Panel on Climate Change (Stocker et al., 2013) attributes to a lack of validation efforts using proxy-based sea-ice reconstructions. Knowledge about (paleo-)sea-ice conditions and ocean temperatures in the climate sensitive areas around the West Antarctic Ice Sheet is hence considered as crucial for understanding past and future climate evolution.

To date, the most common proxy-based sea-ice reconstructions in the Southern Ocean are conducted by the use of sympagic diatom assemblages, which are strongly dependent on their preservation within the sediments (Allen et al., 2011; Armand and Leventer, 2003; Crosta et al., 1998; Esper and Gersonde, 2014; Gersonde and Zielinski, 2000; Leventer, 1998). Dissolution effects within the water column or after deposition determine the preservation state of the small, lightly silicified microfossils and may alter the diatom record, leading to inaccurate sea-ice reconstructions (Leventer, 1998; Zielinski et al., 1998). Recently, the molecular remains of certain diatoms, specific organic geochemical lipids, have emerged as a potential proxy for reconstructing past Antarctic sea-ice cover (Barbara et al., 2013; Collins et al., 2013; Crosta et al., 2021; Denis et al., 2010; Etourneau et al., 2013; Lamping et al., 2020; Massé et al., 2011; Vorrath et al., 2019; 2020). Specifically, a di-unsaturated highly branched isoprenoid (HBI) alkene (HBI diene, $C_{25:2}$) has been detected in both sea-ice diatoms and sediments in the Southern Ocean (Johns et al., 1999; Massé et al., 2011; Nichols et al., 1988), and recently the sympagic (*i.e.* living within sea ice) tube-dwelling diatom *Berkeleya adeliensis* has been identified as producer, which preferably proliferates in platelet ice (Belt et al., 2016; Riaux-Gobin and Poulin, 2004). However, *B. adeliensis* seems rather flexible concerning its habitat, since it was also recorded in the bottom ice layer and seems to be well adapted to changes in texture during ice melt (Riaux-Gobin et al., 2013). Belt et al. (2016) introduced the term $IPSO_{25}$ ("Ice Proxy of the Southern Ocean with 25 carbon atoms") by analogy to the counterpart IP_{25} in the Arctic. Commonly, for a more detailed assessment of sea-ice conditions, IP_{25} in the Arctic Ocean and $IPSO_{25}$ in the Southern Ocean have been measured alongside complementary phytoplankton-derived lipids, such as sterols and/or HBI-trienes, which are indicative of open-water conditions (Belt and Müller, 2013; Lamping et al., 2020; Etourneau et al., 2013; Vorrath

et al., 2019; 2020). The combination of the sea-ice biomarker and a phytoplankton biomarker, the so-called $PIPSO_{25}$ index (Vorrath et al., 2019), allows for a more quantitative differentiation of contrasting sea-ice settings and helps to avoid misinterpretations of the absence of $IPSO_{25}$ which can result from either a lack of sea-ice cover or a permanently thick sea-ice cover, that prevents light penetration hence limiting ice algae growth. Recently, Lamping et al. (2020) used this approach to study changes in sea-ice conditions during the last deglaciation of the Amundsen Sea shelf, which were likely linked to advance and retreat phases of the Getz Ice Shelf.

Multiple mechanisms exist that can cause ice shelf instability. As previously mentioned, relatively warm CDW is considered one of the main drivers for ice shelf thinning in the Amundsen Sea Embayment (Nakayama et al., 2018; Jenkins and Jacobs, 2008; Rignot et al., 2019). Accordingly, changing ocean temperatures are another crucial factor for the stability of the marine-based ice streams draining most of the West Antarctic Ice Sheet (e.g., Colleoni et al., 2018). As for sea-ice reconstructions, organic geochemical lipids for reconstructing ocean temperatures in high latitudes have come into focus in the past decades, since the preservation of calcareous microfossils, which are commonly used for such reconstructions, is very poor in polar marine sediments (e.g., Zamelczyk et al., 2012). Archaeal isoprenoidal glycerol dialkyl glycerol tetraethers (isoGDGTs), sensitive to temperature change and relatively resistant to degradation processes, are well-preserved in marine sediments (Huguet et al., 2008; Schouten et al., 2013). Schouten et al. (2002) found that the number of rings in sedimentary GDGTs is correlated with surface water temperatures and developed the first archaeal lipid paleothermometer TEX_{86}, a ratio of certain GDGTs, as a sea surface temperature (SST) proxy. For polar oceans, Kim et al. (2010) developed a more specific calibration model for temperatures below 15 °C, $TEX^{L}_{86,}$ which employs a different GDGT combination. There is an emerging consensus that GDGTs are rather reflecting subsurface ocean temperatures (SOT) along the Antarctic margin (Kim et al., 2012; Etourneau et al., 2019; Liu et al., 2020). This is supported by observations of elevated archaeal abundances (and GDGTs) in warmer subsurface waters (Liu et al., 2020; Spencer-Jones et al., 2021). Archaea adapt their membrane in cold waters by adding hydroxyl groups and changing the number of rings, OH-GDGTs (Fietz et al., 2020). The additional hydroxyl moieties lead to an increase of the membrane fluidity that aids trans-membrane transport in cold environments, which Huguet et al. (2017)

found in molecular dynamic simulations, explaining the higher relative abundance of OH Archaea lipids in cold environments. Taking the OH-GDGTs into account, Lü et al. (2015) proposed an SST-proxy for the polar oceans, the RI-OH'.

Our aim with this study is to provide insight into the application of biomarkers for sea ice as well as ocean temperature reconstructions in Southern Ocean sediments. Estimates on recent sea-ice coverage and ocean temperatures along the eastern and western Antarctic Peninsula (EAP and WAP) as well as in the Amundsen and Weddell Seas, are based on the analyses of $IPSO_{25}$, HBI-trienes and phytosterols as well as GDGTs in seafloor surface sediment samples from these areas. An intercomparison of biomarker-based sea ice as well as ocean temperature estimates with (1) sea-ice distributions obtained from satellite observations and (2) ocean temperatures deduced from instrumental data allows for an evaluation of the proxy approaches. We further consider AWI-ESM2 climate model data to assess the model's performance in depicting recent oceanic key variables and to examine the potential impact of paleoclimate conditions on the biomarker composition of the investigated surface sediments. In regard of the various factors affecting the use of marine biomarkers as paleoenvironmental proxies, we further comment on the limitations of GDGT temperature estimates and the novel $PIPSO_{25}$ approach, and we discuss the potential connection between $IPSO_{25}$ and platelet ice formation under near-coastal fast ice, which is related to the near-surface presence of sub-ice shelf melt water.

2. Regional setting

The areas of investigation in this study include the southern Drake Passage, the continental shelves of the WAP and EAP (~60° S) and the more southerly located Amundsen and Weddell Seas (~75° S; Fig. 1). The different study areas are all connected by the Antarctic Circumpolar Current (ACC), the Antarctic Coastal Current and the Weddell Gyre (Meredith et al., 2011; Rintoul et al., 2001).

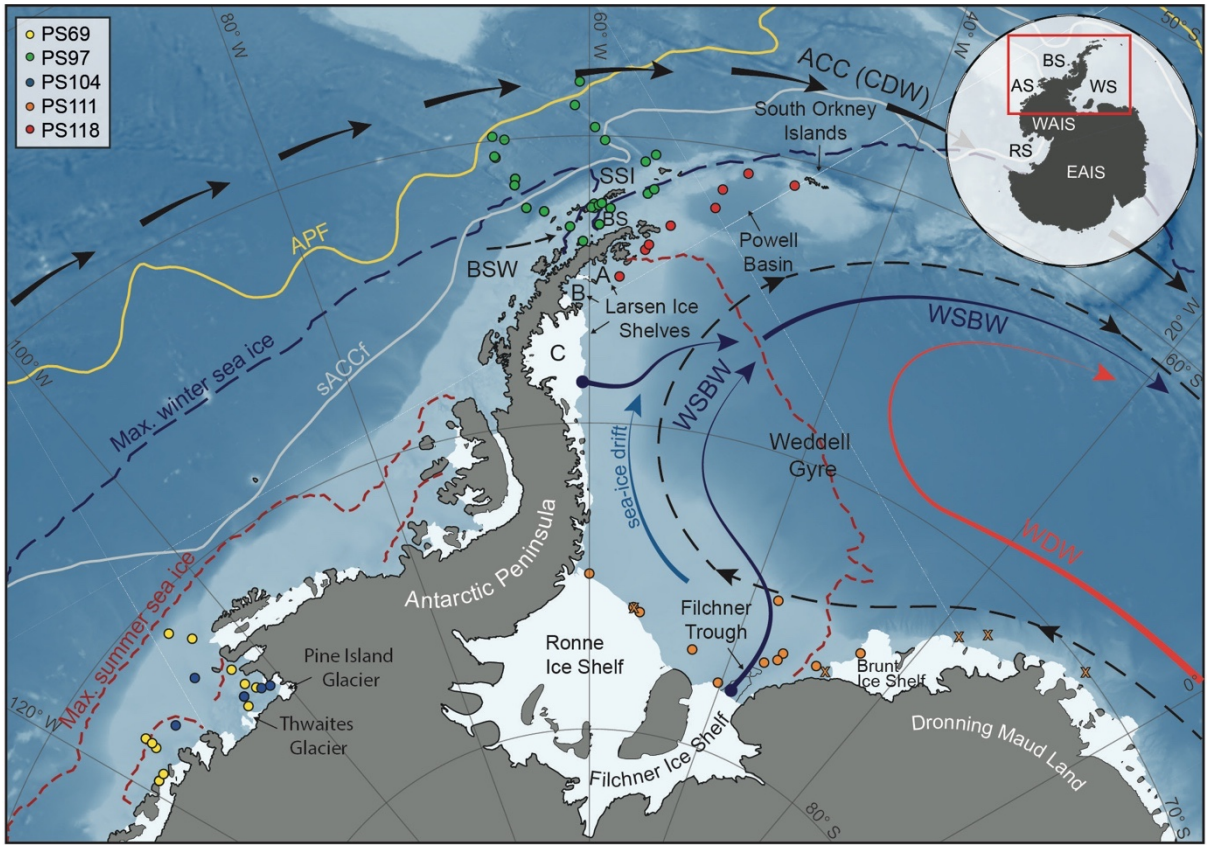

Fig. 1: Map of the study area (location indicated by red box in insert map) including all 41 sample locations (see different colored dots for individual *RV Polarstern* expeditions in the top left corner; for detailed sample information, see Table S1) and main oceanographic features. Maximum summer and winter sea-ice boundaries are marked by dashed red and blue line, respectively (Fetterer et al., 2016). Orange crosses indicate samples where a $PIPSO_{25}$ value of 1 has been assigned due to low biomarker concentrations, close to detection limit. ACC: Antarctic Circumpolar Current, APF: Antarctic Polar Front, sACCf: southern Antarctic Circumpolar Current Front, SSI: South Shetland Islands, BS: Bransfield Strait, BSW: Bellingshausen Sea Water, CDW: Circumpolar Deep Water; WDW: Weddell Deep Water, WSBW: Weddell Sea Bottom Water (Mathiot et al., 2011; Orsi et al., 1995). Insert map shows grounded ice only (i.e., no ice shelves), WAIS: West Antarctic Ice Sheet, EAIS: East Antarctic Ice Sheet, RS: Ross Sea, AS: Amundsen Sea, BS: Bellingshausen Sea, WS: Weddell Sea. Background bathymetry derived from IBCSO data (Arndt et al., 2013).

The ACC is mainly composed of CDW and is the largest current system in the world characterised by a strong eastward flow, which finds its narrowest constriction in the Drake Passage. Along the Bellingshausen Sea, the Amundsen Sea and WAP, where the ACC flows close to the continental shelf edge, CDW is upwelling onto the shelf and flows to the coast via bathymetric troughs, contributing to basal melt and retreat of marine-terminating glaciers and ice shelves (Cook et al., 2016; Jacobs et al., 2011; Jenkins and Jacobs, 2008; Klinck et al., 2004). In the Weddell Sea, a subpolar cyclonic circulation is present south of the ACC, the Weddell Gyre, which deflects part of the ACC's CDW towards the south turning it into Warm Deep Water (WDW; Fig. 1; Hellmer et al., 2016; Vernet et al., 2019). In close vicinity to the Filchner-Ronne and Larsen Ice Shelves, glacially derived freshwater as well as

dense brine released during sea-ice formation contribute to Weddell Sea Bottom Water (WSBW) - a major precursor of Antarctic Bottom Water (Hellmer et al., 2016). Wind and currents force a northward sea-ice drift in the western Weddell Sea along the eastern coast of the Antarctic Peninsula (Harms et al., 2001) until leaving it to melt in warmer waters to the North and up to the Powell Basin (Vernet et al., 2019). At the northern tip of the Antarctic Peninsula, colder and saltier Weddell Sea water masses branch off westwards into the Bransfield Strait where they encounter the well-stratified, warm, and fresh Bellingshausen Sea Water (BSW; Fig. 1), which is entering the Bransfield Strait from the West (Sangrà et al., 2011).

Since 1978, satellite observations show strong seasonal as well as decadal changes in sea-ice cover at the Antarctic Peninsula, which are less pronounced in the more southerly Amundsen and Weddell Seas (Fig. 2a-c). Mean monthly sea-ice concentrations (SIC) for winter (JJA), spring (SON) and summer (DJF) reveal a permanently ice-free Drake Passage, while the WAP and EAP shelf areas are influenced by a changing sea-ice cover in the course of a year (Fig. 2a-c). For the Amundsen and Weddell Seas, satellite data reveal a closed seasonal sea-ice cover with up to ~90 % concentration during winter and spring (Fig. 2a+b), and a late break-up of sea-ice cover to a minimum concentration of ~30 % during summer (Fig. 2c).

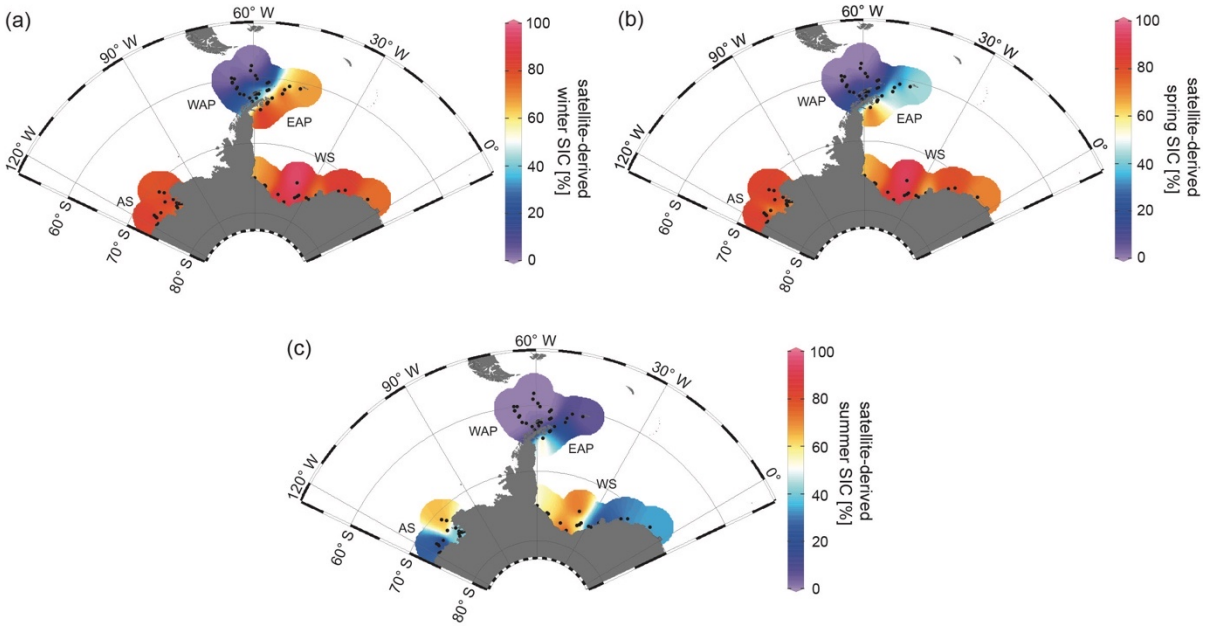

Fig. 2: Distribution of mean monthly satellite-derived sea-ice concentrations for (a) winter (JJA), (b) spring (SON) and (c) summer (DJF) in % (downloaded from the National Snow and Ice Data Center, NSIDC; Cavalieri et al., 1996). AS: Amundsen Sea, WAP: West Antarctic Peninsula, EAP: East Antarctic Peninsula, WS: Weddell Sea.

3. Material and methods

3.1 Sediment samples

In total, we analysed a set of 41 surface sediment samples from different areas of the Southern Ocean (Fig. 1) retrieved by multicorers and giant box corers during *RV Polarstern* expeditions over the past 15 years. Sixteen surface sediment samples from the Amundsen Sea continental shelf were collected during *RV Polarstern* expeditions PS69 in 2006 (Gohl, 2007) and PS104 in 2017 (Gohl, 2017). Twenty-five surface sediment samples from the southeastern and southwestern Weddell Sea continental shelf were collected during *RV Polarstern* expeditions PS111 in 2018 (Schröder, 2018) and PS118 in 2019 (Dorschel, 2019). This set of samples was complemented by 26 surface sediment samples from the Bransfield Strait/WAP for which the analytical results had been previously published by Vorrath et al. (2019).

3.2 Bulk sediment and organic geochemical analyses

The sediment material was freeze-dried and homogenized with an agate mortar and stored in glass vials at -20 °C before and after these initial preparation steps to avoid degradation of targeted molecular components. Total organic carbon (TOC) contents were measured on 0.1 g of sediment after removing inorganic carbon (total inorganic carbon, carbonates) with 500 µl 12 N hydrochloric acid. Measurements were conducted by means of a carbon-sulphur determinator (CS 2000; Eltra) with standards being measured for calibration before sample analyses and after every tenth sample to ensure accuracy (error ± 0.02 %).

Lipid biomarkers were extracted from the sediments (4 g for PS69 and PS104; 6 g for PS111 and PS118) by ultrasonication (3 x 15 min), using dichloromethane:methanol (3 x 6 ml for PS69 and PS104; 3 x 8 ml for PS111 and PS118; 2:1 v/v) as solvent. Prior to this step, the internal standards 7-hexylnonadecane (7-HND; 0.038 µg/sample for PS69 and PS104 and 0.057 µg/sample for PS111 and PS118), 5α-androstan-3-ol (1.04 µg/sample) and C_{46} (0.98 µg/sample) were added to the sample for quantification of HBIs, sterols and GDGTs, respectively. Via open-column chromatography, with SiO_2 as stationary phase, fractionation of the extract was achieved by eluting the apolar fraction (HBIs) and the polar

fraction (sterols and GDGTs) with 5 ml n-hexane and 5 ml DCM/MeOH 1:1, respectively. The polar fraction was subsequently split into two fractions (sterols and GDGTs) for further processing. The sterol fraction was silylated with 300 µl bis-trimethylsilyl-trifluoroacetamide (BSTFA; 2h at 60 °C). Compound analyses of HBIs and sterols were carried out on an Agilent Technologies 7890B gas chromatograph (GC; fitted with a 30 m DB 1MS column; 0.25 mm diameter and 0.25 µm film thickness) coupled to an Agilent Technologies 5977B mass selective detector (MSD; with 70 eV constant ionization potential, ion source temperature of 230 °C). The GC oven was set to: 60 °C (3 min), 150 °C (rate: 15 °C/min), 320 °C (rate: 10 °C/min), 320 °C (15 min isothermal) for the analysis of hydrocarbons and to: 60 °C (2 min), 150 °C (rate: 15 °C/min), 320 °C (rate: 3 °C/min), 320 °C (20 min isothermal) for the analysis of sterols. Helium was used as carrier gas. The identification of HBI and sterol compounds is based upon their GC retention times and mass spectra (Belt, 2018; Belt et al., 2000; Boon et al., 1979). Lipid quantification was obtained by setting the individual, manually integrated, GC-MS peak area in relation to the peak area of the respective internal standard and normalization to the amount of extracted sediment. Quantification of $IPSO_{25}$ and HBI trienes was achieved using their molecular ions ($IPSO_{25}$: m/z 348 and HBI trienes: m/z 346) in relation to the fragment ion m/z 266 of the internal standard 7-HND (Belt, 2018). Quantification of sterols was achieved by comparison of the molecular ion of the individual sterol with the molecular ion m/z 348 of the internal standard 5α-androstan-3-ol. Instrumental response factors for the target lipids were considered as recommended by Belt et al. (2014) and Fahl and Stein (2012). All biomarker concentrations were subsequently normalized to the TOC content of each sample to account for different depositional settings within the different study areas.

For calculating the phytoplankton-$IPSO_{25}$ ($PIPSO_{25}$) index, we used the equation introduced by Vorrath et al. (2019):

$$PIPSO_{25} = IPSO_{25} / (IPSO_{25} + (\text{phytoplankton marker x c})) \quad (1)$$

where c (c = mean $IPSO_{25}$/mean phytoplankton marker) is applied as a concentration balance factor to account for high concentration offsets between $IPSO_{25}$ and the phytoplankton biomarker (see Table S1 for c-factors of individual $PIPSO_{25}$ calculations).

Following the approach by Müller and Stein (2014) and Lamping et al. (2020), samples with exceptionally low (at detection limit) concentrations of both biomarkers have been assigned a $PIPSO_{25}$

187 value of 1 (see chapter 4.1.2). This comprises the five Weddell Seam samples PS111/13-2, /15-1, /16-
188 3, /29-3 and /40-2 (marked as orange x in Fig. 1).
189 The GDGT fraction was dried under N_2, redissolved with 120 µl hexane:isopropanol (v/v 99:1) and
190 then filtered using a polytetrafluoroethylene (PTFE) filter with a 0.45 µm pore sized membrane. GDGT
191 measurements were carried out using high performance liquid chromatography (HPLC; Agilent 1200
192 series HPLC system) coupled to an Agilent 6120 mass spectrometer (MS), operating with atmospheric
193 pressure chemical ionization (APCI). The injection volume was 20 µl. For separating the GDGTs, a
194 Prevail Cyano 3 µm column (Grace, 150 mm * 2.1 mm) was kept at 30 °C. Each sample was eluted
195 isocratically for 5 min with solvent A = hexane/2-propanol/chloroform; 98:1:1 at a flow rate of 0.2
196 ml/min, then the volume of solvent B = hexane/2-propanol/chloroform; 89:10:1 was increased linearly
197 to 10 % within 20 min and then to 100 % within 10 min. The column was back-flushed (5 min, flow
198 0.6 ml/min) after 7 min after each sample and re-equilibrated with solvent A (10 min, flow 0.2 ml/min).
199 The APCI was set to the following: N_2 drying gas flow at 5 l/min and temperature to 350 °C, nebulizer
200 pressure to 50 psi, vaporizer gas temperature to 350 °C, capillary voltage to 4 kV and corona current to
201 +5 µA. Detection of GDGTs was achieved by means of selective ion monitoring (SIM) of $[M+H]^+$ ions
202 (dwell time 76 ms). Determination and quantification of the molecular ions of GDGT-0 (*m/z* 1302),
203 GDGT-1 (*m/z* 1300), GDGT-2 (*m/z* 1298), GDGT-3 (*m/z* 1296) and crenarchaeol (*m/z* 1292) as well as
204 of brGDGT-III (*m/z* 1050), brGDGT-II (*m/z* 1036) and brGDGT-I (*m/z* 1022) was done in relation to
205 the molecular ion *m/z* 744 of the internal standard C_{46}-GDGT. The late eluting hydroxylated GDGTs
206 (OH-GDGT-0, OH-GDGT-1 and OH-GDGT-2 with *m/z* 1318, 1316 and 1314, respectively) were
207 quantified in the scans (*m/z* 1300, 1298, 1296) of their related GDGTs, as described by Fietz et al.
208 (2013).
209 TEX^{L}_{86} values and their conversion into SOTs were determined following Kim et al. (2012):

210 $$TEX_{86}^{L} = LOG\frac{[GDGT-2]}{[GDGT-1]+[GDGT-2]+[GDGT-2]}, \quad (2)$$

211 $$SOT^{TEX}\,[\,°C] \;=\; 50.8\,x\,TEX_{86}^{L} + \;36.1. \quad (3)$$

212 Temperature calculations based on OH-GDGTs were carried out according to Lü et al. (2015):

213 $$RI-OH' = \frac{[OH-GDGT-1]+2\,x\,[OH-GDGT-2]}{[OH-GDGT-0]+[OH-GDGT-1]+[OH-GDGT-2]}, \quad (4)$$

$$SST^{OH}\,[°C] = RI - OH' - 0.1/0.0382\,. \quad (5)$$

To determine the relative influence of terrestrial organic matter input, the Branched Isoprenoid Tetraether (BIT)-index was calculated following Hopmans et al. (2004):

$$BIT = \frac{[brGDGT-I]+[brGDGT-II]+[brGDGT-III]}{[Chrenarchaeol]+[brGDGT-I]+[brGDGT-II]+[brGDGT-III]}\,. \quad (6)$$

3.3 Numerical model

3.3.1 Model description

AWI-ESM2 is a state-of-the-art coupled climate model developed by Sidorenko et al. (2019) which comprises an atmospheric component ECHAM6 (Stevens et al., 2013) as well as an ocean-sea ice component FESOM2 (Danilov et al., 2017). The atmospheric module ECHAM6 is the most recent version of the ECHAM model developed at the Max Planck Institute for Meteorology (MPI) in Hamburg. The model is branched from an early release of the European Center (EC) for Medium Range Weather Forecasts (ECMWF) model (Roeckner et al., 1989). ECHAM6 dynamics is based on hydrostatic primitive equations with traditional approximation. We used a T63 Gaussian grid which has a spatial resolution of about 1.9 x 1.9 degree (1.9 ° or 210 km). There are 47 vertical layers in the atmosphere.

Momentum transport arising from boundary effects is configured using the subgrid orography scheme as described by Lott (1999). Radiative transfer in ECHAM6 is represented by the method described in Iacono et al. (2008). ECHAM6 also contains a Land-Surface Model (JSBACH) which includes 12 functional plant types of dynamic vegetation and 2 bare-surface types (Loveland et al., 2000; Raddatz et al., 2007). The ice-ocean module in AWI-ESM2 is based on the finite volume discretization formulated on unstructured meshes. The multi-resolution for the ocean is up to 15 km over polar and coastal regions, and 135 km for far-field oceans, with 46 uneven vertical depths. The impact of local dynamics on the global ocean is related to a number of FESOM-based studies (Danilov et al., 2017). The multi-resolution approach advocated by FESOM allows one to explore the impact of local processes on the global ocean with moderate computational effort (Danilov et al., 2017). AWI-ESM2 employs the OASIS3-MCT coupler (Valcke, 2013) with an intermediate regular exchange grid.

Mapping between the intermediate grid and the atmospheric/oceanic grid is handled with bilinear interpolation. The atmosphere component computes 12 air–sea fluxes based on four surface fields provided by the ocean module FESOM2. AWI-ESM2 has been validated under modern climate conditions (Sidorenko et al., 2019) and has been applied for marine radiocarbon concentrations (Lohmann et al., 2020), the latest Holocene (Vorrath et al., 2020), and the Last Interglacial (Otto-Bliesner et al., 2021).

3.3.2 Experimental design

One transient experiment was conducted using AWI-ESM2, which applied the boundary conditions, including orbital parameters and greenhouse gases. Orbital parameters are calculated according to Berger (1978), and the concentrations of greenhouse gases are taken from ice-core records as well as from recent measurements of firn air and atmospheric samples (Köhler et al., 2017). The model was initialized from a 1,000-year spin-up run under mid-Holocene (6,000 before present, BP) boundary conditions as described by Otto-Bliesner et al. (2017). In our modeling strategy, we follow Lorenz and Lohmann (2004) and use the climate condition from the mid-Holocene spin-up run as the initial state for the subsequent transient simulation covering the period from 6,000 BP to 2014 CE. In the present study we derived seasonal SIC, SSTs and SOTs in the study area from a segment of the transient experiment (1950-2014 CE). Topography including prescribed ice sheet configuration was kept constant in our transient simulation. All model data are provided in Table S2.

3.4. Satellite SIC and SSTs

Satellite sea-ice data are derived from Nimbus-7 SMMR and DMSP SSM/I-SSMIS passive microwave data and downloaded from the National Snow and Ice Data Center (NSIDC; Cavalieri et al., 1996). The sea-ice data represent mean monthly SIC, which are expressed to range from 0 % to 100 % and are averaged over a period of the beginning of satellite observations in 1978 CE to the individual year of sample retrieval. The monthly mean SIC were then split into different seasons: winter (JJF), spring (SON) and summer (DJF) (Fig. 2a-c) and the data are considered to represent the recent mean state of sea-ice coverage. All satellite data are provided in Table S3.

Modern annual mean SSTs and SOTs are derived from the World Ocean Atlas 13 representing averaged values for the years 1955-2012 CE (WOA13; Locarnini et al., 2013).

4. Results and discussion

In the following, we first present and discuss the biomarker data assembled during this study from North (Antarctic Peninsula) to South (Amundsen and Weddell Seas) and draw conclusions about the environmental settings deduced from the data set. As phytoplankton-derived biomarkers, we here focus on the significance of HBI Z-triene and brassicasterol, while HBI E-triene and dinosterol - showing very similar patterns - are moved to the supplement (Fig. S1) to avoid repetition. All biomarker data collected during this study are provided in Table S1 and are available via the PANGAEA data repository (in prep.). For the discussion of the target environmental variables, *i.e.* $PIPSO_{25}$-based sea ice and GDGT-derived ocean temperature estimates, satellite and instrumental as well as modelled data are considered. In Sect. 5, we further address potential caveats in biomarker-based environmental reconstructions that need to be considered when applying these proxies.

4.1 TOC content, HBIs and sterols in Antarctic surface sediments

TOC contents in marine sediments in a first approximation are often viewed as an indicator for primary productivity in surface waters (Meyers, 1997). However, we are aware that additional factors, such as different water depths or depositional regimes, may exert control on sedimentary TOC as well. The TOC contents of the herein investigated surface samples are lowest in Drake Passage with values around 0.12-0.54 %, increasing in a northwest-southeast gradient into Bransfield Strait, ranging between 0.59 and 1.06 % (Fig. 3a; WAP). At the EAP, higher TOC contents (0.57-0.86 %) prevail around the Larsen Ice Shelf with a decreasing trend towards the Powell Basin (0.22-0.37 %) and an increase to 0.50 % around the area of the South Orkney Islands, which may point to elevated productivity or enhanced supply of reworked terrigenous organic matter in these areas (Fig. 3a; EAP).

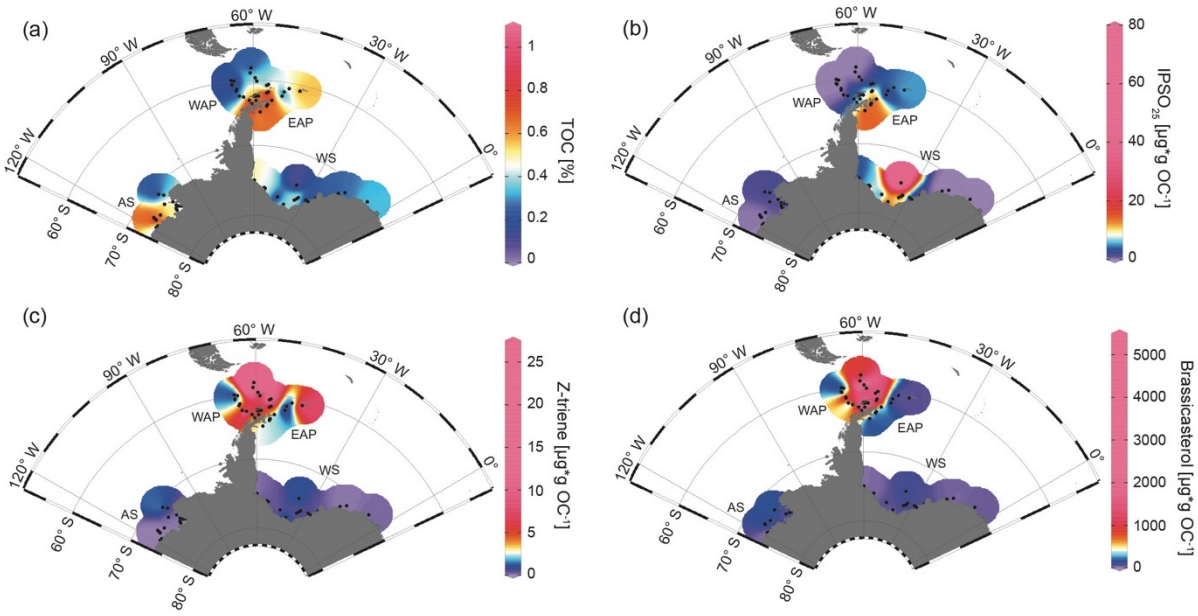

Fig. 3: Distribution of (a) TOC [%], (b) $IPSO_{25}$, (c) Z-triene and (d) brassicasterol in surface sediment samples. Sample locations are marked as black dots. Concentrations of biomarkers [µg*g OC^{-1}] were normalized to the TOC content of each sample. AS: Amundsen Sea, WAP: West Antarctic Peninsula, EAP: East Antarctic Peninsula, WS: Weddell Sea.

At the WAP, concentrations of the sea-ice biomarker $IPSO_{25}$ show a northwest-southeast gradient with $IPSO_{25}$ being absent in samples from the permanently ice-free Drake Passage and increasing concentrations towards the continental slope and the seasonally ice-covered continental shelf (0.37-17.81 µg*g OC^{-1}; Fig. 3b; Vorrath et al., 2019). Highest $IPSO_{25}$ concentrations are observed in samples of the northern Bransfield Strait, which is affected by inflow of water masses from the Weddell Sea through the Antarctic Sound and along the Antarctic Peninsula and frequent transport of sea ice into the Bransfield Strait (Vorrath et al., 2019). Elevated $IPSO_{25}$ concentrations are also observed at the EAP, influenced by a seasonal sea-ice cover, where relatively higher concentrations of the sea-ice biomarker prevail in those samples located in front of the Larsen Ice Shelf (12.59-17.74 µg*g OC^{-1}; Fig. 3b). As these locations are also influenced by the northward drift of sea ice within the Weddell Gyre (Fig. 1), the elevated $IPSO_{25}$ concentrations could also result from sea ice advected from the southern Weddell Sea. We suggest that the decreasing $IPSO_{25}$ concentrations towards the Powell Basin and the South Orkney Islands (0.59-5.36 µg*g OC^{-1}; Fig. 3b) can be connected to warmer ocean temperatures towards the North and less sea-ice coverage during spring.

Concentrations of the phytoplankton biomarker HBI Z-triene around the Antarctic Peninsula are highest in the eastern Drake Passage and along the continental slope (where $IPSO_{25}$ is absent) and decrease in the Bransfield Strait (0.33-26.86 μg*g OC^{-1}; Fig. 3c; Vorrath et al., 2019). Elevated HBI Z-triene concentrations have thus far been detected in surface waters along an ice edge (Smik et al., 2016) and hence suggested to be a proxy for marginal ice zone conditions (Belt et al., 2015; Collins et al., 2013; Schmidt et al., 2018). Vorrath et al. (2019), however, relate the high concentrations of HBI Z-triene at the northernmost stations in the permanently ice-free eastern Drake Passage to their proximity to the Antarctic Polar Front. Here, productivity of the source diatoms of HBI-trienes (*e.g.*, *Rhizosolenia* spp.; Belt et al., 2017) may be enhanced by meander-induced upwelling leading to increased nutrient flux to surface waters (Moore and Abbott, 2002). Since Cardenas et al. (2019) document only minor abundances of *Rhizosolenia* spp. in surface sediments from this area, we assume that HBI-trienes might also be biosynthesized by other diatoms. Moderate concentrations along the continental slope of the WAP and in the Bransfield Strait have been associated with elevated inflow of warm BSW which leads to a retreating sea-ice margin during spring and summer (for more details, see Vorrath et al., 2019; 2020). Samples from the EAP continental shelf and the Powell Basin are characterised by relatively low concentrations of HBI Z-triene (Fig. 3c; 0.1-2.37 μg*g OC^{-1}), showing a southwest-northeast gradient, while the northernmost sample closest to the South Orkney Islands is characterized by an elevated HBI Z-triene concentration of ~8.49 μg*g OC^{-1} (Fig. 3c; EAP). This relatively high concentration may be related to an "Island Mass Effect", coined by Doty and Oguri (1956), which refers to an increased primary production around oceanic islands in comparison to surrounding waters. Nolting et al. (1991) found extraordinarily high dissolved iron levels (as high as 50-60 nM) on the shelf of the South Orkney Islands, and Nielsdóttir et al. (2012) observed enhanced iron and Chl *a* concentrations in the vicinity of the South Orkney Islands. These authors explain the increased dissolved iron levels with input from seasonally retreating sea ice, which is recorded by satellites (Fig. 2a-c) and probably leads to substantial annual phytoplankton blooms, which may also cause the elevated TOC content in the corresponding seafloor sediment sample (Fig. 3a). Alternatively, remobilization of shelf sediments or vertical mixing of iron-rich deep waters leading to high iron contents in surface waters may stimulate primary productivity (Blain et al., 2007; de Jong et al., 2012). However, it remains unclear why the

336 brassicasterol concentration is distinctly low in this sample, and we assume that different environmental
337 preferences of the source organisms may account for this. In Drake Passage and the EAP, brassicasterol
338 displays a similar pattern as the HBI Z-triene, with relatively high concentrations (more than 2 orders
339 of magnitudes), ranging between 1.86 and 5017.44 µg*g OC^{-1} (Fig. 3d).
340 In the Weddell Sea, TOC contents are generally lower (< 0.4 %), with slightly elevated values in the
341 West (up to 0.50 %) and right in front of the Filchner Ice Shelf (up to 0.52 %; Fig. 3a). The Amundsen
342 Sea is characterized by slightly higher TOC contents, with concentrations of up to 0.91 % in the West
343 and lower values in the East (0.33 %; Fig. 3a; AS).
344 In the samples from the Amundsen and Weddell Seas, dominated by a strong winter sea-ice cover
345 lasting until spring (Fig. 2a-c), all three biomarkers are present in low concentrations only. An exception
346 are the samples located in front of the Filchner Ice Shelf with significantly higher concentrations of
347 $IPSO_{25}$ (7.09-73.87 µg*g OC^{-1}; Fig. 3b; WS). Concentrations of $IPSO_{25}$ on the Amundsen Sea shelf are
348 relatively low (0.04-3.3 µg*g OC^{-1}), with slightly higher values observed towards the north-east (Fig.
349 3b; AS). HBI Z-triene is also very low concentrated, showing slightly higher concentrations in Filchner
350 Trough (0.04-1 µg*g OC^{-1}) and towards the more distal locations in the northeastern Amundsen Sea
351 (0.01-1.88 µg*g OC^{-1}; Fig. 3c). Brassicasterol generally shows similar patterns as the HBI Z-triene,
352 with concentrations ranging between 1.86 and 220.54 µg*g OC^{-1} (Fig. 3d; for HBI E-triene and
353 dinosterol distribution, see Fig. S1).
354
355 4.2 Combining individual biomarker records: the $PIPSO_{25}$ index
356 The $PIPSO_{25}$ index combines the relative concentrations of $IPSO_{25}$ and a selected phytoplankton
357 biomarker, such as HBI-trienes and sterols, as indicator for an open-ocean environment (Vorrath et al.,
358 2019). The combination of both end members (sea ice vs. open-ocean) prevents misleading
359 interpretations regarding the absence of $IPSO_{25}$ in the sediments, which can be the result of two entirely
360 different scenarios. At heavy/perennial sea-ice conditions, the thickness of sea ice hinders light
361 penetration, thereby limiting the productivity of algae living in basal sea ice (Hancke et al., 2018). This
362 scenario may cause the absence of both phytoplankton and sea-ice biomarkers in the sediment. The
363 other scenario depicts a permanently open ocean, where the sea-ice biomarker is absent as well, but

here, the phytoplankton biomarkers are present in variable concentrations (Müller et al., 2011). The presence of both biomarkers in the sediment is indicative of seasonal sea-ice coverage and/or the occurrence of stable sea-ice margin conditions, promoting biosynthesis of both biomarkers (Müller et al., 2011). We here distinguish between P_ZIPSO_{25} and P_BIPSO_{25} using HBI Z-triene and brassicasterol as phytoplankton biomarker, respectively (Fig. 4a+b; for $PIPSO_{25}$ values based on HBI E-triene and dinosterol see Table S1 and Fig. S2).

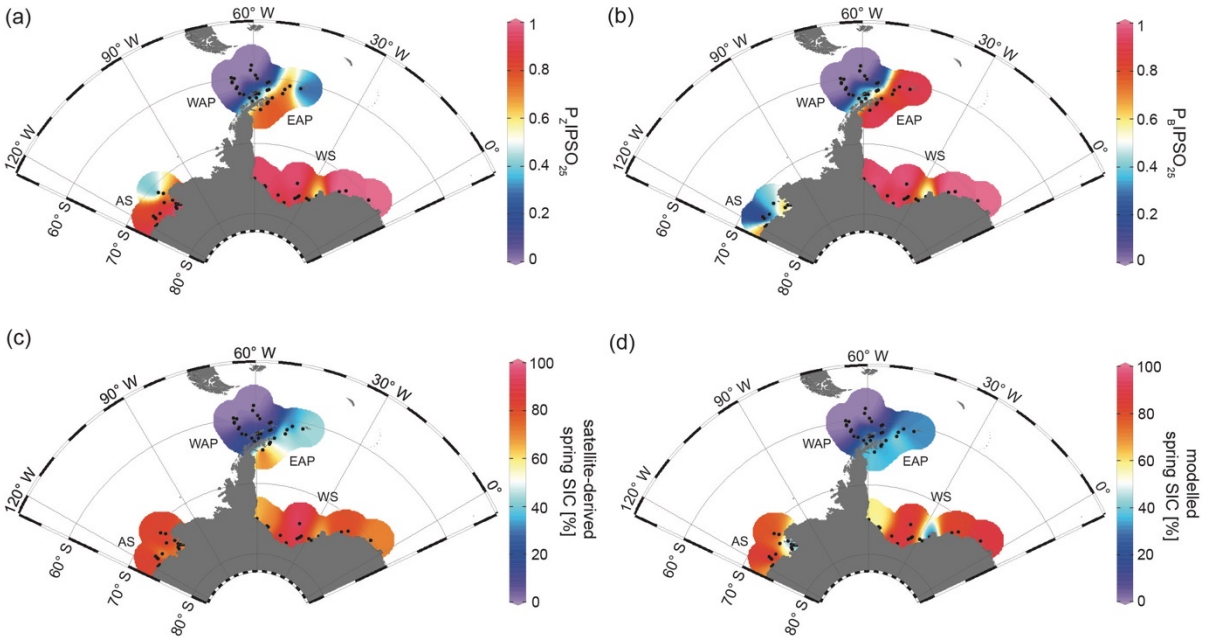

Fig. 4: Distribution of the sea-ice index $PIPSO_{25}$ in surface sediment samples, with (a) P_ZIPSO_{25} based on Z-triene and (b) P_BIPSO_{25} based on brassicasterol, (c) satellite-derived spring SIC [%] and (d) modelled spring SIC [%]. AS: Amundsen Sea, WAP: West Antarctic Peninsula, EAP: East Antarctic Peninsula, WS: Weddell Sea.

Both $PIPSO_{25}$ indices are 0 in the predominantly ice-free Drake Passage and display a northwest-southeast gradient to intermediate values towards the continental slope and the South Shetland Islands, reflecting increased influence of marginal sea-ice cover towards the coast (0.02-0.70; Vorrath et al., 2019). At the seasonally sea-ice covered EAP, P_ZIPSO_{25} values reach 0.84, while lower values of around 0.25 are observed close to the South Orkney Islands, which relates to the elevated HBI Z-triene concentrations at the stations there (Fig. 3c; EAP). The P_BIPSO_{25} index exhibits even higher values of up to 0.98 at the EAP/northwestern Weddell Sea. These elevated $PIPSO_{25}$ indices align well with the significant northward ice-drift within the Weddell Gyre in that region, which leads to prolonged sea-ice cover along the EAP.

In samples from the southern Weddell Sea, both $PIPSO_{25}$ indices show a similar pattern with high values up to 0.9, and slightly lower values in front of the Brunt Ice Shelf (0.6; Fig. 4a+b). Very low concentrations (close to detection limit) of both biomarkers in samples located on the continental shelf off Dronning Maud Land (Fig. 1) result in low $PIPSO_{25}$ values, strongly underestimating the sea-ice cover in that area. Regarding the satellite-derived sea-ice data, this area of the continental shelf is influenced by a severe seasonal sea-ice cover (Fig. 2). As previously mentioned, we followed the approach by Müller and Stein (2014) and Lamping et al. (2020) and assigned a maximum $PIPSO_{25}$ value of 1 to these samples to circumvent misleading interpretations and aid visualisation.

The intermediate $PIPSO_{25}$ value (~0.51) derived for one sample collected in front of the Brunt Ice Shelf points to a less severe sea-ice cover in that area. A possible explanation for the relatively lower $PIPSO_{25}$ value may be the presence of a coastal polynya that has been reported by Anderson (1993) and which is further supported by Paul et al. (2015), who note that the sea-ice area around the Brunt Ice Shelf is the most active in the southern Weddell Sea, with an annual average polynya area of 3516 ± 1420 km². Interestingly, the reduced SIC here is also captured by our model (see Sect. 4.3).

$PIPSO_{25}$ values in the Amundsen Sea point to different scenarios. The P_ZIPSO_{25} index ranges around 0.9 with only the easterly, more distal locations showing lower values between 0.3 and 0.6 (Fig. 4a). The P_BIPSO_{25} index generally presents lower values ranging from 0.6 in the coastal area to 0.2 in the more distal samples (Fig. 4b). This difference between P_ZIPSO_{25} and P_BIPSO_{25} may be explained by the different source organisms biosynthesizing the individual phytoplankton biomarkers. While the main origin of HBI-trienes seems to be restricted to diatoms (Belt et al., 2017), brassicasterol is known to be produced by several algal groups adapted to a wider range of sea surface conditions (Volkman, 2006; see Sect. 5.2).

4.3 Biomarker-based sea ice estimates vs. satellite and model data

The main ice algae bloom in the Southern Ocean occurs during spring, when solar insolation and air temperatures/SSTs increase and sea ice starts melting, which results in the release of nutrients and stratification of the water column stimulating the productivity of photosynthesizing organisms (Arrigo, 2017; Belt, 2018). The sea-ice biomarker $IPSO_{25}$ is hence commonly interpreted as a spring sea-ice

407 indicator, which is why, in the following, we compare the biomarker-based sea-ice reconstructions to
408 satellite-derived and modelled spring SIC. $IPSO_{25}$ concentrations in the surface sediments around the
409 Antarctic Peninsula exhibit similar trends as the satellite-derived and modelled SIC (Figs. 3+4), while
410 they differ significantly in the Amundsen and Weddell Seas, where high SIC are depicted by satellites
411 and the model but $IPSO_{25}$ is very low concentrated. The low $IPSO_{25}$ concentrations in these areas
412 highlight the uncertainty when considering $IPSO_{25}$ as a sea-ice proxy alone, since such low
413 concentrations are not only observed under open water conditions, but also under a severe sea-ice cover.
414 In this case, the low concentrations of $IPSO_{25}$ are the result of the latter, where limited light availability
415 hinders ice algae growth, leading to an underestimation of sea-ice cover. Accordingly, we note a weak
416 correlation between $IPSO_{25}$ data and satellite SIC ($R^2 = 0.19$; Fig. 5a). As stated above, the combination
417 of $IPSO_{25}$ and a phytoplankton marker may prevent this ambiguity. The higher sea-ice concentrations
418 in the Amundsen and Weddell Seas are better reflected by maximum P_ZIPSO_{25} values than by $IPSO_{25}$
419 alone. However, we note that the P_ZIPSO_{25} index seems to not further resolve SICs higher than 50 %
420 (see Fig. S3), which may indicate a threshold (here ~50 % SIC) where the growth of the HBI triene and
421 $IPSO_{25}$ producing algae is limited.

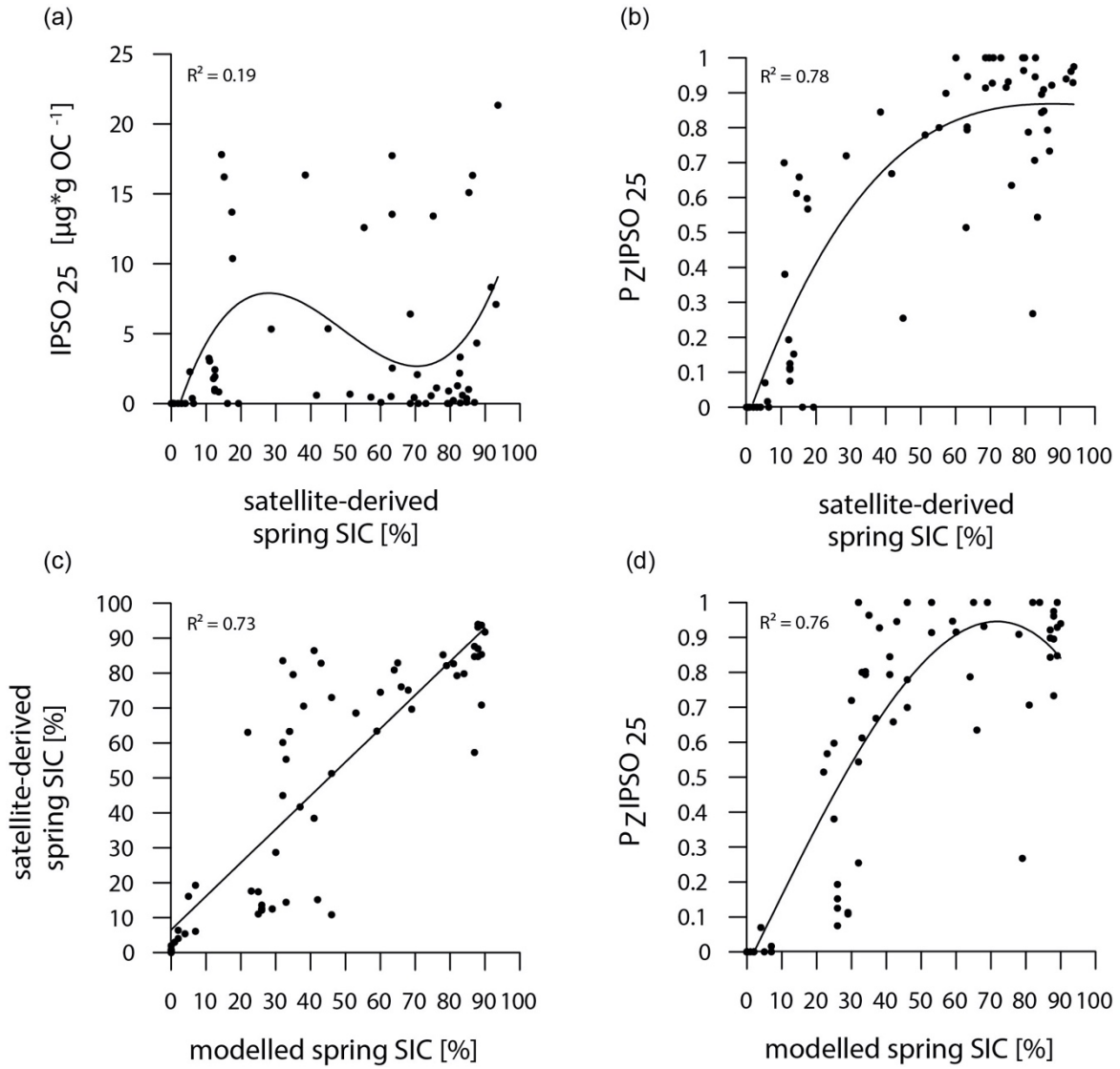

Fig. 5: Correlations of (a) $IPSO_{25}$ concentrations vs. satellite-derived spring SIC, (b) P_ZIPSO_{25} values vs. satellite-derived spring SIC, (c) satellite-derived spring SIC vs. modelled spring SIC and (d) P_ZIPSO_{25} values vs. modelled spring SIC. Coefficients of determination (R^2) are given for the respective regression lines.

In general, however, the P_ZIPSO_{25} values correlate much better with satellite and modelled SIC (R^2 = 0.78 and R^2 = 0.76, respectively; Fig. 5b+d) than $IPSO_{25}$ concentrations. Correlations of satellite and model data with $PIPSO_{25}$ calculated using the HBI E-triene, brassicasterol and dinosterol, respectively, are also positive but less significant (Fig. S4) and we hence focus the discussion on P_ZIPSO_{25}.The AWI-ESM2-derived spring SICs correctly display the permanently ice-free Drake Passage and the northwest-southeast gradient in sea-ice cover from the WAP continental slope towards the Bransfield Strait (Fig. 4d). The model, however, significantly underestimates the elevated sea-ice concentrations (up to 70 %) in front of the former Larsen Ice Shelf A and east of James Ross Island at the EAP depicted by satellite

data. In the Amundsen and Weddell Seas, the model shows a heavy sea-ice cover (~90 %), only slightly underestimating the sea-ice cover at the near-coastal sites in front of Pine Island Glacier and the Ronne Ice Shelf. Interestingly, modelled SIC in the area in front of the Brunt Ice Shelf is as low as ~45 % (Fig. 4d+e), corresponding well with the reduced P_ZIPSO_{25} value of ~0.51, and may reflect the polynya conditions in that region documented by Anderson (1993) and Paul et al. (2015). Overall, we note that modelled modern SICs correlate well with satellite data ($R^2 = 0.73$; Fig. 5c) and P_ZIPSO_{25} values ($R^2 = 0.76$; Fig. 5d), while we observe weaker correlations between modelled paleo-SICs and P_ZIPSO_{25} values (Fig. S5; see Sect. 5.1).

4.4 TEX^L_{86}- and RI-OH'- derived ocean temperatures

For a critical appraisal of the applicability and reliability of GDGT indices as temperature proxies in polar latitudes, we here focus on the TEX^L_{86} proxy by Kim et al. (2012), potentially reflecting SOTs, and the RI-OH' proxy, assumed to reflect SSTs, by Lü et al. (2015). The reconstructions are considered to represent annual mean ocean temperatures (for correlations of TEX^L_{86}-derived SOTs with WOA spring and winter SOTs, see Fig. S6). In all samples, the BIT-index (Eq. 6) is <0.3, indicating no significant contribution of terrestrial input influencing the distribution and hence applicability of GDGTs to estimate ocean temperatures. RI-OH'-derived temperatures and TEX^L_{86}-derived SOTs both show a similar pattern, but different temperatures ranging between -2.62 to +4.67 °C and -2.38 to +8.75 °C, respectively (Fig. 6a+b). At the WAP, RI-OH'- as well as TEX^L_{86}-derived temperatures follow a northwest-southeast gradient with higher temperatures in the permanently ice-free Drake Passage and on the Antarctic continental slope, influenced by the ACC and relatively warm CDW (Orsi et al., 1995; Rintoul et al., 2001). Temperatures decrease towards the Bransfield Strait and the EAP, which are influenced by a seasonal sea-ice cover and relatively colder and highly saline water from the Weddell Sea, branching off the Weddell Gyre (Collares et al., 2018; Thompson et al., 2009). At the EAP, a southwest-northeast gradient can be observed with relatively lower temperatures along the

455 Larsen Ice Shelf and higher temperatures towards the Powell Basin and the South Orkney Islands (Fig.
456 6a+b).

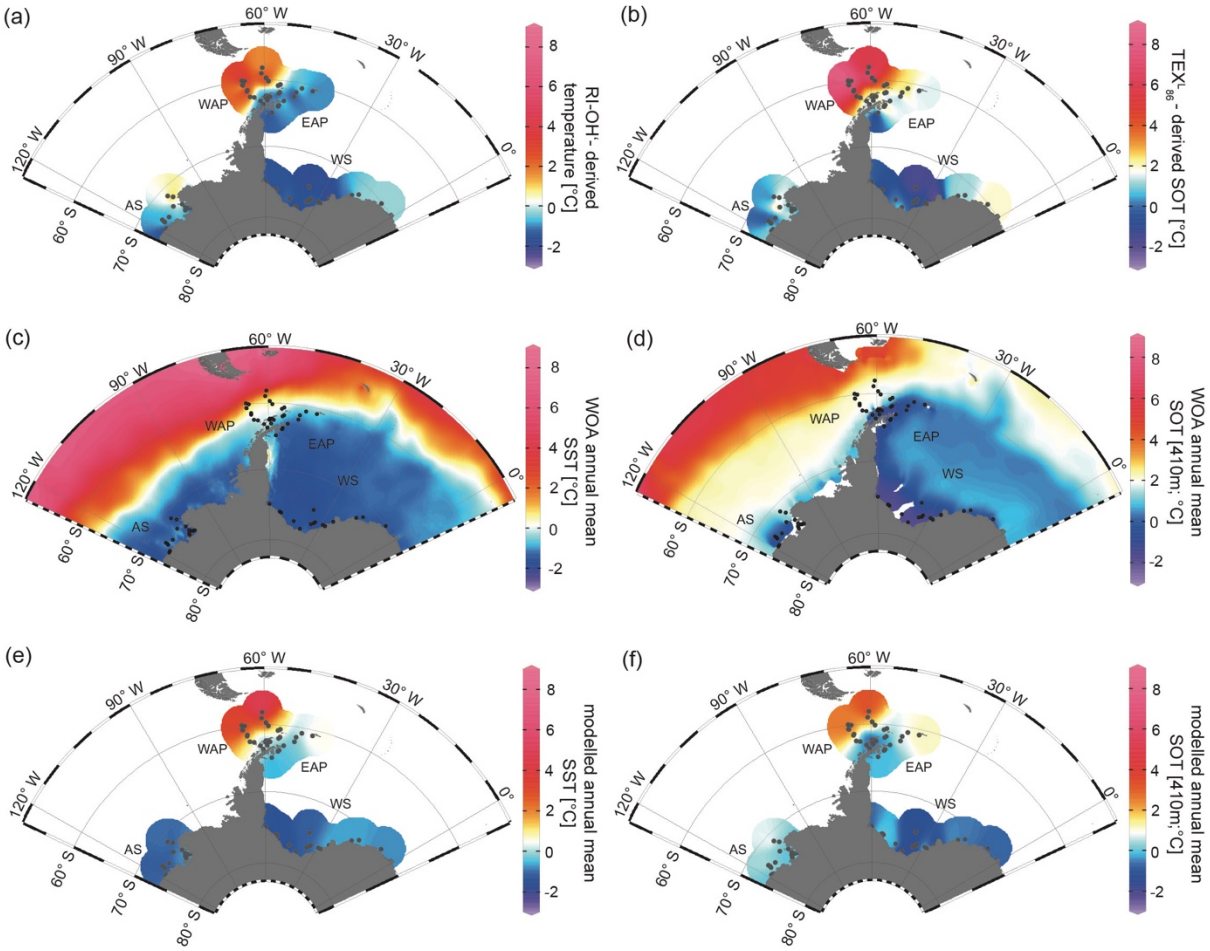

Fig. 6: Annual mean temperature distributions with (a) RI-OH´-derived temperature, (b) TEX^{L}_{86}-derived SOT, (c) WOA13 SST (Locarnini et al., 2013), (d) WOA13 SOT (410 m; Locarnini et al., 2013), (e) modelled SST and (f) modelled SOT (410 m) in °C. AS: Amundsen Sea, WAP: West Antarctic Peninsula, EAP: East Antarctic Peninsula, WS: Weddell Sea.

457 Further to the South, in the Amundsen and Weddell Seas, temperatures are generally lower than at the
458 Antarctic Peninsula. Samples from the Weddell Sea display a temperature decrease from east to west,
459 which may reflect the eddy-driven route in the north-eastern corner of the Weddell Gyre carrying
460 relatively warm, salty CDW, which then advects westward along the southern edge of the Weddell Gyre
461 as WDW (Vernet et al., 2019). Coldest TEX^{L}_{86} as well as RI-OH' temperatures (<0 °C) at sites along
462 the Filchner-Ronne Ice Shelf front may be further linked to the presence of cold precursor water masses
463 for WSBW.

With regard to ongoing discussions, whether GDGT-based temperature reconstructions represent SSTs or SOTs (Kalanetra et al., 2009; Kim et al., 2012; Park et al., 2019), we here compare our RI-OH' and TEX^{L}_{86}-derived temperatures with instrumental and modelled surface as well as subsurface temperature data (Fig. 6c-f). Based on correlations of GDGT-derived temperatures with WOA13 temperatures reflecting different water depths, we observe the highest significance at a water depth of 410 m (for respective correlations, see Fig. S7). When discussing instrumental and modelled SOTs, we hence refer to 410 m water depth.

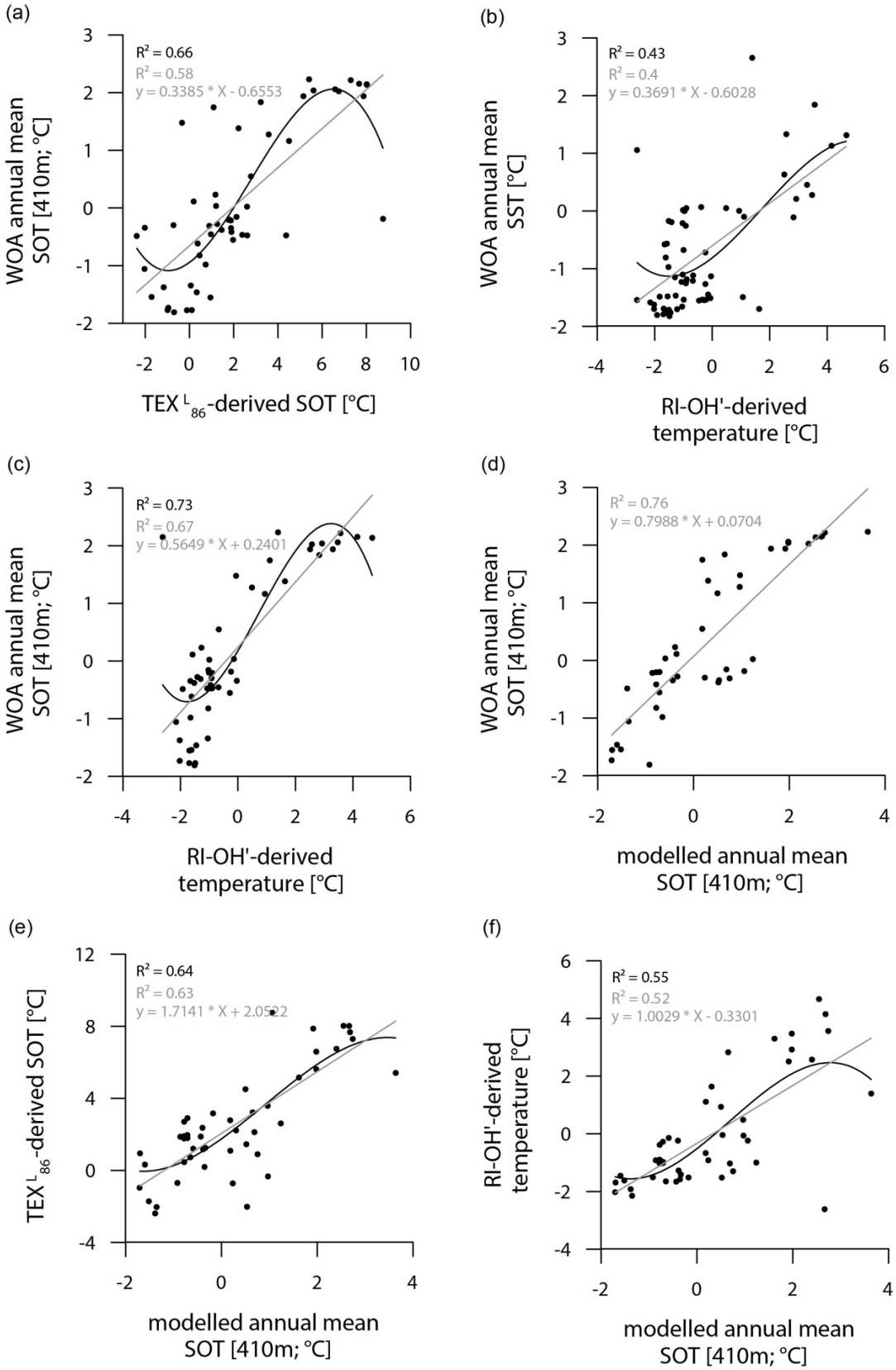

Fig. 7: Correlations of (a) WOA annual mean SOT (410 m) vs. TEX^{L}_{86}-derived SOT, (b) WOA annual mean SST vs. RI-OH'-derived temperature, (c) WOA annual mean SOT (410 m) vs. RI-OH'-derived temperature, (d) WOA annual mean SOT (410 m) vs. modelled annual mean SOT (410 m), (e) TEX^{L}_{86}-derived SOT vs. modelled annual mean SOT (410 m), (f) RI-OH'-derived temperature vs. modelled annual mean SOT (410 m) in °C. Coefficients of determination (R^2) are given for the respective regression lines.

While the correlation between TEX^{L}_{86}-derived SOTs and instrumental SOTs is reasonably well (Fig. 7a; R^2 = 0.66), also supporting the assumption of a subsurface origin, we note a significant overestimation of SOTs by up to 6 °C in the Drake Passage (Fig. S8). This warm-biased TEX^{L}_{86} signal is a known caveat and is, among others, assumed to be connected to GDGTs produced by deep-dwelling Euryarchaeota (Park et al., 2019), which have been reported in CDW (Alonso-Sáez et al., 2011) and in deep waters at the Antarctic Polar Front (López-García et al., 2001). Maximum TEX^{L}_{86}-based SOTs of 5 °C - 8 °C in the central Drake Passage (Fig. 6b), however, distinctly exceed the common temperature range of CDW (0-2 °C). Interestingly, TEX^{L}_{86}-derived SOTs in the colder regions of the Amundsen and Weddell Seas relate reasonably well to instrumental temperatures and are only slightly warm-biased (Fig. S8). Correlations between RI-OH'-derived temperatures with instrumental SSTs are comparatively weak (R^2 = 0.43; Fig. 7b). Recently, Liu et al. (2020) concluded in their study on surface sediments from Prydz Bay (East Antarctica), that also the RI-OH' index holds promise as a tool to reconstruct SOTs rather than SSTs. When correlating our RI-OH'-derived temperatures with instrumental SOTs, we find a high correlation (R^2 = 0.73; Fig. 7c), too, supporting this hypothesis. We further note that the temperature range of RI-OH' is much more realistic than TEX^{L}_{86}, supporting the study by Park et al. (2019) and demonstrating that the addition of OH-isoGDGTs in the temperature index is a promising step towards high latitude temperature reconstructions and may improve our understanding of the temperature responses of archaeal membranes in Southern Ocean waters (Fietz et al., 2020; Park et al., 2019). Clearly, more data – ideally obtained from sediment traps, surface samples as well as longer sediment cores – and calibration studies will help to further elucidate the applicability of this approach.

Similar to the model-derived sea-ice data, we here also evaluate the model's performance in depicting ocean temperatures (Fig. 6e+f). Modelled annual mean SSTs and SOTs are highest with up to 5 °C and 3 °C, respectively, in the permanently ice-free Drake Passage, influenced by the relatively warm ACC. Decreasing SSTs are simulated towards the Antarctic Peninsula continental slope and the Bransfield Strait (~0.5 to 1 °C), coinciding with the increase in the duration of seasonal sea-ice cover in that area. At the EAP/northwestern Weddell Sea, modelled SSTs as well as SOTs show a southwest-northeast

directed increase towards Powell Basin. In the Amundsen and Weddell Seas, annual mean SSTs are negative, with temperatures ranging from -1 to -0.5 °C, while SOTs are positive in the Amundsen Sea and negative in the Weddell Sea. Overall, we note that modelled SOTs reflect instrumental SOTs reasonably well (R^2 = 0.76; Fig. 7d). Interestingly, while RI-OH'-derived SOTs relate better to instrumental SOTs (than TEX^L_{86}-based SOTs), we note a better correlation between TEX^L_{86}-derived SOTs and modelled SOTs (R^2 = 0.64; Fig. 7e) and a weaker correlation with Ri-OH'-derived temperatures (R^2 = 0.55; Fig. 7f).

5. Caveats and recommendations for future research

Marine core top studies to elucidate the applicability of climate proxies are often concerned with limitations and uncertainties regarding the age control of the investigated surface sediments as well as the production, preservation and degradation of target compounds. In the following, we shortly address some of these factors and provide brief recommendations for future investigations.

5.1 Age control

Information on the actual age of the surface sediments are a major requirement determining their suitability to reflect modern sea surface conditions. When comparing sea-ice conditions or ocean temperatures estimated from sedimentary biomarker data (easily spanning decades to millennia, depending on sedimentation rates) with satellite-derived sea-ice data or instrumental records (covering only the past ~40 and 65 years, respectively), the different time periods reflected in the data sets need to be considered when interpreting the results. To address the issue of lacking age constraints for the herein studied surface sediments, we also performed paleoclimate simulations providing sea-ice concentration data for three time slices (2 ka, 4 ka and 6 ka BP; see Fig. S5) to evaluate, if the surface sediments may have recorded significantly older environmental conditions. Correlations of $PIPSO_{25}$ values against these paleo time slice sea-ice concentrations depicted notably weaker relations (Fig. S5) compared to the recent (1951-2014 CE) model output, which points to a relatively young age of the majority of the herein studied sediments. This is further supported by AMS ^{14}C-dating of calcareous

525 microfossils and ^{210}Pb-dating of seafloor surface sediments from the Amundsen Sea shelf documenting
526 recent ages for most sites (Hillenbrand et al., 2010, 2013, 2017; Smith et al., 2011, 2014, 2017; Witus
527 et al., 2014) as well as modern ^{210}Pb-dates obtained for three multicores collected in the Bransfield
528 Strait (PS97/56, PS97/68, PS97/72; Vorrath et al., 2020), which are considered in this study, too. AMS
529 ^{14}C dates obtained for nearby surface samples in the vicinity of the South Shetland Islands and the
530 Antarctic Sound revealed ages of 100 years and 142 years BP, respectively (Vorrath et al., 2019). As
531 both uncorrected ages lie within the range of the modern marine reservoir effect (e.g. Gordon and
532 Harkness, 1992), we may consider these two dates still modern. However, in an area that is significantly
533 affected by rapid climate warming over the past decades and a regionally variable sea ice coverage,
534 uncertainties associated with ^{14}C dating of calcareous material may easily lead to an over- or
535 underestimation of biomarker-based sea-ice cover and ocean temperature estimates, respectively, which
536 needs to be considered for comparisons with instrumental data. While the utilization of (paleo) model
537 data may alleviate the lack of age control for each seafloor sediment sample to some extent, we
538 accordingly recommend that for a robust calibration of *e.g.* $PIPSO_{25}$ values against satellite-derived sea-
539 ice concentrations (and this is not the aim of this study) only surface sediment samples with a modern
540 age confirmed by ^{210}Pb-dating are incorporated.
541
542 5.2 Production and preservation of biomarkers
543 Biomarkers are considered to reveal the former occurrence of their precursor organisms, which requires
544 a certain source specificity. While there is general consensus on *e.g.* Thaumarchaeota being the major
545 source for iso-GDGTs (Fietz et al., 2020 and references therein) or diatoms synthesizing HBIs
546 (Volkman 2006), this is not the case for brassicasterol, which is not only found in diatoms but also in
547 *e.g.* dinoflagellates and haptophytes (Volkman 2006). Accordingly, the use of brassicasterol to
548 determine the $PIPSO_{25}$ index may introduce uncertainties regarding the environmental information
549 pertinent to this phytoplankton biomarker. A further aspect concerns the different chemical structures
550 of HBIs and sterols, which raises the risk of a selective degradation (see Belt, 2018 and Rontani et al.,
551 2018; 2019 for detailed discussion) with potentially considerable effects on the $PIPSO_{25}$ index.
552 Regarding the different sectors of the study area, also spatially different microbial communities as well

as varying depositional regimes, such as sedimentation rate, redox conditions and water depth, may lead to different degradation patterns, which means that variations in the biomarker concentrations between different sectors may not strictly reflect changes in the production of these compounds (driven by sea surface conditions) but may also relate to different degradation states. In particular, lower sedimentation rates and thus extended oxygen exposure times promote chemical alteration and degradation processes (Hedges et al., 1990; Schouten et al., 2013). Regarding the transport of organic matter from the sea surface through the water column, it has been previously noted that the formation of mineral aggregates and fecal pellets, however, often accelerates the vertical export towards the seafloor during the melting season leading to a more rapid burial and hence better preservation (Bauerfeind et al., 2005; Etourneau et al., 2019; Müller et al., 2011).

Another rather technical drawback concerning the use of the $PIPSO_{25}$ index may appear when the concentrations of the sea-ice proxy $IPSO_{25}$ and the phytoplankton marker are similarly low (due to unfavourable conditions for both ice algae as well as phytoplankton) or similarly high (due to a significant seasonal shift in sea-ice cover and/or stable ice edge conditions). This may lead to similar $PIPSO_{25}$ values, although the sea-ice conditions are fundamentally different from each other. This scenario occurred at five sampling sites in the Weddell Sea (PS111/13-2, /15-1, /16-3, /29-3, and /40-2; Fig. 3b+c), where $IPSO_{25}$ and the HBI Z-triene concentrations are close to the detection limit and P_ZIPSO_{25} values are very low, suggesting a reduced sea-ice cover. Satellite and model data, however, show that these sample locations are influenced by heavy, nearly year-round sea-ice cover. We conclude that biomarker concentrations of both biomarkers at or close to the detection limit, indicative of a severe ice cover, need to be treated with caution. As mentioned above, we assigned a maximum P_ZIPSO_{25} value of 1 to these samples and we note that such practice always needs to be made clear when applying the $PIPSO_{25}$ approach. The coupling of $IPSO_{25}$ with a phytoplankton marker, nonetheless, provides more reliable sea-ice reconstructions. Regarding the above-mentioned ambiguities, we recommend not only to calculate the $PIPSO_{25}$ index, but also to carefully consider individual biomarker concentrations and, if possible, to utilize other sea-ice measures, such as well-preserved diatom assemblage data (Lamping et al., 2020; Vorrath et al., 2019; 2020). While the $PIPSO_{25}$ index is not yet a fully quantitative proxy to provide paleo sea-ice concentrations, the GDGT-paleothermometers have gone through several

calibration iterations (Fietz et al., 2020). As noted above, the observation of distinctly warm-biased TEX^{L}_{86}-derived SOTs calls for further efforts in terms of regional calibration studies and/or investigations of archaean adaptation strategies regarding different water depths, nutrient and temperature conditions.

5.3 The role of platelet ice for the production of $IPSO_{25}$

The sympagic, tube-dwelling, diatom *B. adeliensis* is a common constituent of Antarctic sea ice, preferably flourishing in the relatively open channels of sub-ice platelet layers in near-shore locations covered by fast ice (Medlin, 1990; Riaux-Gobin and Poulin, 2004). Based on investigations of sea-ice samples from the Southern Ocean, Belt et al. (2016) detected this diatom species to be a source of $IPSO_{25}$, which, according to its habitat, led to the assumption of the sea-ice proxy being a potential indicator for the presence of platelet ice. As stated above, *B. adeliensis* is not confined to platelet ice, but is also observed in basal sea ice and described as well adapted to changes in the texture of sea ice during ice melt (Riaux-Gobin et al., 2013). Platelet ice formation, however, plays an important role in sea-ice generation along some coastal regions of Antarctica (Hoppmann et al., 2015; 2020; Lange et al., 1989; Langhorne et al., 2015). In these regions, CDW and High Saline Shelf Water (HSSW) flowing into sub-ice shelf cavities of ice shelves cause basal melting and the discharge of cold and less saline water (Fig. 8; Hoppmann et al., 2020, Scambos et al., 2017). The surrounding water is cooled and freshened and is then transported towards the surface. Under the large Filchner-Ronne and Ross ice shelves the pressure relief can cause this water, called Ice Shelf Water (ISW), to be supercooled (Foldvik and Kvinge, 1974). The temperature of the supercooled ISW is potentially below the in-situ freezing point, which may eventually cause the formation of ice platelets that accumulate under landfast ice attached to adjacent ice shelves (Fig. 8; Holland et al., 2007; Hoppmann et al., 2015; 2020).

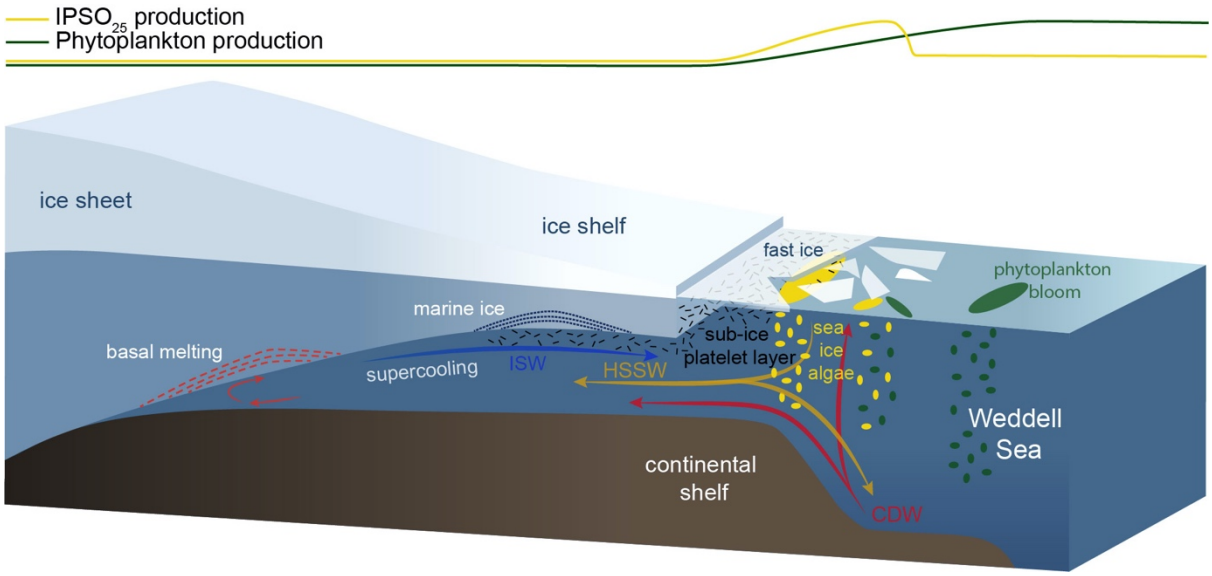

Fig. 8: Schematic illustration of the formation of platelet ice and the main production areas of sea ice algae producing $IPSO_{25}$ (yellow ovals) and phytoplankton (green ovals), also displayed by yellow and green curves at the top. CDW: Circumpolar Deep Water, HSSW: High Saline Shelf Water, ISW: Ice Shelf Water. Schematic modified after Scambos et al. (2017).

In an attempt to elucidate the relationship of $IPSO_{25}$ and platelet ice more clearly, we here regard our data in connection to observed platelet ice occurrences.

While the maximum $IPSO_{25}$ concentrations in front of the Filchner Ice Shelf could be directly related to the above-mentioned platelet ice formation in this area, the elevated $IPSO_{25}$ concentrations in front of the Larsen Ice Shelves at the EAP could be linked to several processes. According to Langhorne et al. (2015), sea-ice cores retrieved from that area did not incorporate platelet ice. The high $IPSO_{25}$ concentrations could hence be explicable by either input from drift ice transported with the Weddell Gyre or by basal freeze-on. We do, however, note that our samples may reflect much longer time frames than the sea-ice samples investigated by Langhorne et al. (2015) and the lack of platelet ice in their investigated sea-ice cores does not rule out the former presence of platelet ice, which may be captured in our investigated sediment samples.

There are several previous studies on $IPSO_{25}$ which report a close connection of the proxy to proximal, coastal locations and polynyas in the seasonal ice zone (i.e., Collins et al., 2013; Smik et al., 2016). They do not, however, discuss the relation to adjacent ice shelves as possible “platelet ice factories”. We note that the core locations investigated by Smik et al. (2016) are in the vicinity of the Moscow University Ice Shelf, where Langhorne et al. (2015) did not observe platelet ice within sea-ice cores.

620 Hoppmann et al. (2020), however, report a sea-ice core from that area, which incorporates platelet ice.
621 The different observations by Langhorne et al. (2015) and Hoppmann et al. (2020) highlight the
622 temporal variability in the occurrence of platelet ice in the cold water regime around the East Antarctic
623 margin.
624 Regarding the minimum abundance of $IPSO_{25}$ in the Amundsen Sea (Fig. 3b; AS), which we tentatively
625 relate to the extended and thick sea ice coverage, the absence of platelet ice in that region may be an
626 alternative explanation. The Amundsen/Bellingshausen Sea and WAP shelves are classified as warm
627 shelves (Thompson et al., 2018) characterized by the upwelling of warm CDW (Schmidtko et al., 2014),
628 hindering the formation of ISW and making the presence of platelet ice in recent conditions highly
629 unlikely (Hoppmann et al., 2020). This theory is also supported by Langhorne et al. (2015), stating that
630 platelet ice formation is not observed, where thinning from basal melting of ice shelves is believed to
631 be greatest, which applies to the warm West Antarctic continental shelf in the eastern Pacific sector of
632 the Southern Ocean (Thompson et al., 2018). Accordingly, if the formation and accumulation of platelet
633 ice – up to a certain degree – is indicative of basal ice shelf melting on fresh shelves (Hoppmann et al.,
634 2015; Thompson et al., 2018), high $IPSO_{25}$ concentrations determined in marine sediments may hence
635 serve as indicator of ISW formation and associated ice shelf dynamics. This may, however, only be true
636 up to a certain threshold where platelet ice formation is diminished/hampered due to warm oceanic
637 conditions causing too intense sub-ice shelf melting (Langhorne et al., 2015).
638 While using $IPSO_{25}$ as a sea-ice proxy in Antarctica, it is hence important to also consider regional
639 platelet ice formation processes as these may affect the $IPSO_{25}$ budget. Determining thresholds
640 associated with platelet ice formation is challenging. Therefore, further investigations, such as in-situ
641 measurements of $IPSO_{25}$ concentrations in platelet ice or culture experiments in home laboratories, are
642 needed to better depict the connection between $IPSO_{25}$ and platelet ice formation (and ice shelf basal
643 melting).
644

645 **7. Conclusions**

646 Biomarker analyses focusing on $IPSO_{25}$, HBI-trienes, phytosterols and GDGTs in surface sediment
647 samples from the Antarctic continental margin were investigated to depict recent sea ice conditions and

ocean temperatures in this climate sensitive region. Proxy-based reconstructions of these key variables were compared to (1) satellite sea-ice data, (2) instrumental ocean temperature data as well as (3) modelled sea-ice patterns and ocean temperatures. The semi-quantitative sea-ice index $PIPSO_{25}$, combining the sea-ice proxy $IPSO_{25}$ with an open-water phytoplankton marker, yielded reasonably good correlations with satellite observations and numerical model results, while correlations with the sea-ice proxy $IPSO_{25}$ alone are rather low. Minimum concentrations of both biomarkers, used for the $PIPSO_{25}$ calculations, however, may lead to ambiguous interpretations and significant underestimations of sea-ice conditions. Different sea-ice measures when interpreting biomarker data should hence be considered.

Ocean temperature reconstructions based on the TEX^{L}_{86-} and RI-OH'-paleothermometers show similar patterns, but different absolute temperatures. While TEX^{L}_{86}-derived temperatures are significantly biased towards warm temperatures in Drake Passage, the RI-OH'-derived temperature range seems more realistic, when compared to temperature data based on the WOA13 and modelled annual mean SOTs.

Further investigations of HBI- as well as GDGT-synthesis, transport, sedimentation and preservation within the sediments would help to guide the proxies' application. Further taxonomy work, the composition of the $IPSO_{25}$ producer's habitat (basal sea ice, platelet ice, brine channels) and its connection to platelet ice formation via in situ or laboratory measurements are required to better constrain the $IPSO_{25}$ potential as a robust sea-ice biomarker. The presumed relationship between $IPSO_{25}$ and platelet ice formation in connection to basal melting of ice shelves is supported by our data, showing high $IPSO_{25}$ concentrations in areas where platelet ice formation has previously been reported and low $IPSO_{25}$ concentrations where no platelet ice formation is observed. Accordingly, oceanic conditions and the intensity of sub-ice shelf melting need to be considered when using $IPSO_{25}$ (1) as an indirect indicator for sub-ice shelf melting processes and associated ice shelf dynamics and (2) for the application of the $PIPSO_{25}$ index to estimate sea ice coverage.

Data availability

Datasets related to this article can be found online on *PANGAEA Data Publisher for Earth & Environmental Science* (doi: in prep).

Author contribution

N.L. and J.M. designed the concept of the study. N.L. carried out biomarker experiments. X.S and G.L. developed the model code and X.S. performed the simulations. C.H. provided the satellite data. M.-E.V. provided hitherto unpublished GDGT data for PS97 samples. G.M. and J.H. carried out GDGT analyses. C.-D.H. collected surface sediment samples and advised on their ages. N.L. prepared the manuscript and visualizations with contributions from all co-authors.

Competing interests

The authors declare that they have no conflict of interest.

Acknowledgements

Denise Diekstall, Mandy Kuck and Jonas Haase are kindly acknowledged for laboratory support. We thank the captains, crews and science parties of *RV Polarstern* cruises PS69, PS97, PS104, PS111 and PS118. Especially, Frank Niessen, Sabine Hanisch and Michael Schreck are thanked for their support during PS118. Simon Belt is acknowledged for providing the 7-HND internal standard for HBI quantification. AWI, MARUM - University of Bremen, the British Antarctic Survey and NERC UK-IODP are acknowledged for funding expedition PS104. N.L., M.-E.V. and J.M. were funded through the Helmholtz Research Grant VH-NG-1101. Two anonymous reviewers are thanked for their constructive and helpful comments, which lead to a distinct improvement of this manuscript.

References

Abernathey, R. P., Cerovecki, I., Holland, P. R., Newsom, E., Mazloff, M., and Talley, L. D.: Water-mass transformation by sea ice in the upper branch of the Southern Ocean overturning, Nature Geoscience, 9, 596-601, 2016.

Allen, C. S., Pike, J., and Pudsey, C. J.: Last glacial–interglacial sea-ice cover in the SW Atlantic and its potential role in global deglaciation, Quaternary Science Reviews, 30, 2446-2458, 2011.

Alonso-Sáez, L., Andersson, A., Heinrich, F., and Bertilsson, S.: High archaeal diversity in Antarctic circumpolar deep waters, Environmental microbiology reports, 3, 689-697, 2011.

Anderson, P. S.: Evidence for an Antarctic winter coastal polynya, Antarctic science, 5, 221-226, 1993.

Armand, L. K., and Leventer, A.: Palaeo sea ice distribution–reconstruction and palaeoclimatic significance, Sea ice—an introduction to its physics, biology, chemistry, and geology, 333-372, 2003.

Arrigo, K. R., Worthen, D. L., Lizotte, M. P., Dixon, P., and Dieckmann, G.: Primary production in Antarctic sea ice, Science, 276, 394-397, 1997.

Arrigo, K. R.: Sea ice as a habitat for primary producers, Sea ice, 352-369, 2017.

Barbara, L., Crosta, X., Massé, G., and Ther, O.: Deglacial environments in eastern Prydz Bay, East Antarctica, Quaternary Science Reviews, 29, 2731-2740, 2010.

Barbara, L., Crosta, X., Schmidt, S., and Massé, G.: Diatoms and biomarkers evidence for major changes in sea ice conditions prior the instrumental period in Antarctic Peninsula, Quaternary Science Reviews, 79, 99-110, 2013.

Bauerfeind, E., Leipe, T. and Ramseier, R.O.: Sedimentation at the permanently ice-covered Greenland continental shelf (74°57.7'N/12°58.7'W): significance of biogenic and lithogenic particles in particulate matter flux. Journal of Marine Systems 56, 151-166, 2005.

Belt, S. T., Allard, W. G., Massé, G., Robert, J.-M., and Rowland, S. J.: Highly branched isoprenoids (HBIs): identification of the most common and abundant sedimentary isomers, Geochimica et Cosmochimica Acta, 64, 3839-3851, 2000.

Belt, S. T., and Müller, J.: The Arctic sea ice biomarker IP_{25}: a review of current understanding, recommendations for future research and applications in palaeo sea ice reconstructions, Quaternary Science Reviews, 79, 9-25, 2013.

Belt, S. T., Brown, T. A., Ampel, L., Cabedo-Sanz, P., Fahl, K., Kocis, J. J., Masse, G., Navarro-Rodriguez, A., Ruan, J., and Xu, Y.: An inter-laboratory investigation of the Arctic sea ice

biomarker proxy IP_{25} in marine sediments: key outcomes and recommendations, Climate of the Past., 10, 155-166, 2014.

Belt, S. T., Cabedo-Sanz, P., Smik, L., Navarro-Rodriguez, A., Berben, S. M. P., Knies, J., and Husum, K.: Identification of paleo Arctic winter sea ice limits and the marginal ice zone: Optimised biomarker-based reconstructions of late Quaternary Arctic sea ice, Earth and Planetary Science Letters, 431, 127-139, 2015.

Belt, S. T., Smik, L., Brown, T. A., Kim, J. H., Rowland, S. J., Allen, C. S., Gal, J. K., Shin, K. H., Lee, J. I., and Taylor, K. W. R.: Source identification and distribution reveals the potential of the geochemical Antarctic sea ice proxy $IPSO_{25}$, Nature Communications, 7, 12655, https://doi.org/10.1038/ncomms12655, 2016.

Belt, S. T., Brown, T. A., Smik, L., Tatarek, A., Wiktor, J., Stowasser, G., Assmy, P., Allen, C. S., and Husum, K.: Identification of C_{25} highly branched isoprenoid (HBI) alkenes in diatoms of the genus Rhizosolenia in polar and sub-polar marine phytoplankton, Organic Geochemistry, 110, 65-72, 2017.

Belt, S. T.: Source-specific biomarkers as proxies for Arctic and Antarctic sea ice, Organic Geochemistry, 125, 277-298, 2018.

Berger, A.: Long-term variations of daily insolation and Quaternary climatic changes, Journal of the atmospheric sciences, 35, 2362-2367, 1978.

Blain, S., Quéguiner, B., Armand, L., Belviso, S., Bombled, B., Bopp, L., Bowie, A., Brunet, C., Brussaard, C., Carlotti, F., Christaki, U., Corbière, A., Durand, I., Ebersbach, F., Fuda, J.-L., Garcia, N., Gerringa, L., Griffiths, B., Guigue, C., Guillerm, C., Jacquet, S., Jeandel, C., Laan, P., Lefèvre, D., Lo Monaco, C., Malits, A., Mosseri, J., Obernosterer, I., Park, Y.-H., Picheral, M., Pondaven, P., Remenyi, T., Sandroni, V., Sarthou, G., Savoye, N., Scouarnec, L., Souhaut, M., Thuiller, D., Timmermans, K., Trull, T., Uitz, J., van Beek, P., Veldhuis, M., Vincent, D., Viollier, E., Vong, L. and Wagener, T.: Effect of natural iron fertilization on carbon sequestration in the Southern Ocean. Nature 446, 1070-1074, 2007.

Boon, J. J., Rijpstra, W. I. C., de Lange, F., De Leeuw, J., Yoshioka, M., and Shimizu, Y.: Black Sea sterol—a molecular fossil for dinoflagellate blooms, Nature, 277, 125-127, 1979.

Cavalieri, D., Parkinson, C., Gloersen, P., and Zwally, H.: Sea ice concentrations from Nimbus-7 SMMR and DMSP SSM/I passive microwave data, National Snow and Ice Data Center, Boulder, Colorado, USA, 1996.

Collares, L. L., Mata, M. M., Kerr, R., Arigony-Neto, J., and Barbat, M. M.: Iceberg drift and ocean circulation in the northwestern Weddell Sea, Antarctica, Deep Sea Research Part II: Topical Studies in Oceanography, 149, 10-24, 2018.

Colleoni, F., De Santis, L., Siddoway, C. S., Bergamasco, A., Golledge, N. R., Lohmann, G., Passchier, S., and Siegert, M. J.: Spatio-temporal variability of processes across Antarctic ice-bed–ocean interfaces, Nature Communications, 9, 2289, https://doi.org/10.1038/s41467-018-04583-0, 2018.

Collins, L. G., Allen, C. S., Pike, J., Hodgson, D. A., Weckström, K., and Massé, G.: Evaluating highly branched isoprenoid (HBI) biomarkers as a novel Antarctic sea-ice proxy in deep ocean glacial age sediments, Quaternary Science Reviews, 79, 87-98, 2013.

Comiso, J. C., Gersten, R. A., Stock, L. V., Turner, J., Perez, G. J., and Cho, K.: Positive Trend in the Antarctic Sea Ice Cover and Associated Changes in Surface Temperature, Journal of Climate, 30, 2251-2267, 2017.

Cook, A.J., Holland, P., Meredith, M., Murray, T., Luckman, A., Vaughan, D.G.: Ocean forcing of glacier retreat in the WAP. Science, 353, 283-286, 2016.

Crosta, X., Pichon, J. J., and Burckle, L.: Application of modern analog technique to marine Antarctic diatoms: Reconstruction of maximum sea-ice extent at the Last Glacial Maximum, Paleoceanography and Paleoclimatology, 13, 284-297, 1998.

Crosta, X., Etourneau, J., Orme, L.C., Dalaiden, Q., Campagne, P., Swingedouw, D., Goosse, H., Massé, G., Miettinen, A., McKay, R.M., Dunbar, R.B., Escutia, C. and Ikehara, M.: Multi-decadal trends in Antarctic sea-ice extent driven by ENSO–SAM over the last 2,000 years. Nature Geoscience 14, 156-160, 2021.

Danilov, S., Sidorenko, D., Wang, Q., and Jung, T.: The Finite-volumE Sea ice–Ocean Model (FESOM2), Geosci. Model Dev., 10, 765-789, 2017.de Jong, J., Schoemann, V., Lannuzel, D., Croot, P., de Baar, H. and Tison, J.-L.: Natural iron fertilization of the Atlantic sector of the

786 Southern Ocean by continental shelf sources of the Antarctic Peninsula. Journal of Geophysical
787 Research: Biogeosciences 117, 2012.
788 Denis, D., Crosta, X., Barbara, L., Massé, G., Renssen, H., Ther, O., and Giraudeau, J.: Sea ice and
789 wind variability during the Holocene in East Antarctica: insight on middle–high latitude coupling,
790 Quaternary Science Reviews, 29, 3709-3719, 2010.
791 Dorschel, B.: The Expedition PS118 of the Research Vessel POLARSTERN to the Weddell Sea in
792 2019, Berichte zur Polar-und Meeresforschung = Reports on polar and marine research, 735,
793 2019.
794 Doty, M. S., and Oguri, M.: The island mass effect, ICES Journal of Marine Science, 22, 33-37,
795 1956.
796 Eayrs, C., Li, X., Raphael, M.N. and Holland, D.M.: Rapid decline in Antarctic sea ice in recent
797 years hints at future change. Nature Geoscience 14, 460-464, 2021.
798 Esper, O., and Gersonde, R.: New tools for the reconstruction of Pleistocene Antarctic sea ice,
799 Palaeogeography, Palaeoclimatology, Palaeoecology, 399, 260-283, 2014.
800 Etourneau, J., Collins, L. G., Willmott, V., Kim, J.-H., Barbara, L., Leventer, A., Schouten, S.,
801 Damsté, J. S., Bianchini, A., and Klein, V.: Holocene climate variations in the WAP: evidence
802 for sea ice extent predominantly controlled by changes in insolation and ENSO variability,
803 Climate of the Past, 9, 1431-1446, 2013.
804 Etourneau, J., Sgubin, G., Crosta, X., Swingedouw, D., Willmott, V., Barbara, L., Houssais, M.-N.,
805 Schouten, S., Damsté, J.S.S., Goosse, H.: Ocean temperature impact on ice shelf extent in the
806 eastern Antarctic Peninsula. Nature Communications 10, 1-8, 2019.
807 Fahl, K., and Stein, R.: Modern seasonal variability and deglacial/Holocene change of central Arctic
808 Ocean sea-ice cover: new insights from biomarker proxy records, Earth and Planetary Science
809 Letters, 351, 123-133, 2012.
810 Fetterer, F., Knowles, K., Meier, W., Savoie, M., Windnagel, A.K., 2016. Updated Daily. Sea Ice
811 Index, Version 2. [Median Sea Ice Extent 1981-2010]. NSIDC: National Snow and Ice Data
812 Center, Boulder, Colorado USA. https://doi.org/10.7265/N5736NV7 [24 July 2017].

Fietz, S., Huguet, C., Rueda, G., Hambach, B., and Rosell-Melé, A.: Hydroxylated isoprenoidal GDGTs in the Nordic Seas, Marine Chemistry, 152, 1-10, 2013.

Fietz, S., Ho, S., and Huguet, C.: Archaeal Membrane Lipid-Based Paleothermometry for Applications in Polar Oceans, Oceanography, 33, 104-114, 2020.

Foldvik, A., and Kvinge, T.: Conditional instability of sea water at the freezing point, Deep Sea Research and Oceanographic Abstracts, 21, 169-174, 1974.

Fretwell, P., Pritchard, H.D., Vaughan, D.G., 57 others. Bedmap2: improved ice bed, surface and thickness datasets for Antarctica. Cryosphere 7, 375-393. http://dx.doi.org/10.5194/tc-7-375-2013, 2013.

Gersonde, R., and Zielinski, U.: The reconstruction of late Quaternary Antarctic sea-ice distribution—the use of diatoms as a proxy for sea-ice, Palaeogeography, Palaeoclimatology, Palaeoecology, 162, 263-286, 2000.

Gohl, K.: The expedition ANTARKTIS-XXIII/4 of the research vessel Polarstern in 2006, Berichte zur Polar-und Meeresforschung (Reports on Polar and Marine Research), 557, 2007.

Gohl, K.: The Expedition PS104 of the Research Vessel POLARSTERN to the Amundsen Sea in 2017, Berichte zur Polar-und Meeresforschung = Reports on polar and marine research, 712, 2017.

Gordon, J.E., Harkness, D.D.: Magnitude and geographic variation of the radiocarbon content in Antarctic marine life: implications for reservoir corrections in radiocarbon dating, Quaternary Science Reviews 11, 697-708, 1992.

Hancke, K., Lund-Hansen, L. C., Lamare, M. L., Højlund Pedersen, S., King, M. D., Andersen, P., and Sorrell, B. K.: Extreme low light requirement for algae growth underneath sea ice: A case study from Station Nord, NE Greenland, Journal of Geophysical Research: Oceans, 123, 985-1000, 2018.

Harms, S., Fahrbach, E., and Strass, V. H.: Sea ice transports in the Weddell Sea, Journal of Geophysical Research: Oceans, 106, 9057-9073, 2001.

Hedges, J.I., Hu, F.S., Devol, A.H., Hartnett, H.E., Tsamakis, E. and Keil, R.G.: Sedimentary organic matter preservation; a test for selective degradation under oxic conditions. Am J Sci 299, 529-555, 1999.

Hellmer, H.H., Rhein, M., Heinemann, G., Abalichin, J., Abouchami, W., Baars, O., Cubasch, U., Dethloff, K., Ebner, L., Fahrbach, E., Frank, M., Gollan, G., Greatbatch, R.J., Grieger, J., Gryanik, V.M., Gryschka, M., Hauck, J., Hoppema, M., Huhn, O., Kanzow, T., Koch, B.P., König-Langlo, G., Langematz, U., Leckebusch, G.C., Lüpkes, C., Paul, S., Rinke, A., Rost, B., van der Loeff, M.R., Schröder, M., Seckmeyer, G., Stichel, T., Strass, V., Timmermann, R., Trimborn, S., Ulbrich, U., Venchiarutti, C., Wacker, U., Willmes, S. and Wolf-Gladrow, D.: Meteorology and oceanography of the Atlantic sector of the Southern Ocean - a review of German achievements from the last decade. Ocean Dynamics 66, 1379-1413, 2016.

Hillenbrand, C.-D., Smith, J.A., Kuhn, G., Esper, O., Gersonde, R., Larter, R.D., Maher, B., Moreton, S.G., Shimmield, T.M., Korte, M.: Age assignment of a diatomaceous ooze deposited in the western Amundsen Sea Embayment after the Last Glacial Maximum. Journal of Quaternary Science 25, 280-295, 2010.

Hillenbrand, C.-D., Kuhn, G., Smith, J.A., Gohl, K., Graham, A.G.C., Larter, R.D., Klages, J.P., Downey, R., Moreton, S.G., Forwick, M., Vaughan, D.G.: Grounding-line retreat of the West Antarctic Ice Sheet from inner Pine Island Bay. Geology 41, 35-38, 2013.

Hillenbrand, C.-D., Smith, J.A., Hodell, D.A., Greaves, M., Poole, C.R., Kender, S., Williams, M., Andersen, T.J., Jernas, P.E., Elderfield, H., Klages, J.P., Roberts, S.J., Gohl, K., Larter, R.D., Kuhn, G.: West Antarctic Ice Sheet retreat driven by Holocene warm water intrusions. Nature 547, 43–48, 2017.

Ho, S. L., Mollenhauer, G., Fietz, S., Martínez-Garcia, A., Lamy, F., Rueda, G., Schipper, K., Méheust, M., Rosell-Melé, A., Stein, R., and Tiedemann, R.: Appraisal of TEX_{86} and thermometries in subpolar and polar regions, Geochimica et Cosmochimica Acta, 131, 213-226, 2014.

Hobbs, W. R., Massom, R., Stammerjohn, S., Reid, P., Williams, G., and Meier, W.: A review of recent changes in Southern Ocean sea ice, their drivers and forcings, Global and Planetary Change, 143, 228-250, 2016.

Holland, P. R., Feltham, D. L., and Jenkins, A.: Ice shelf water plume flow beneath Filchner-Ronne Ice Shelf, Antarctica, Journal of Geophysical Research: Oceans, 112, https://doi.org/10.1029/2006JC003915, 2007.

Hopmans, E. C., Weijers, J. W., Schefuß, E., Herfort, L., Damsté, J. S. S., and Schouten, S.: A novel proxy for terrestrial organic matter in sediments based on branched and isoprenoid tetraether lipids, Earth and Planetary Science Letters, 224, 107-116, 2004.

Hoppmann, M., Nicolaus, M., Paul, S., Hunkeler, P. A., Heinemann, G., Willmes, S., Timmermann, R., Boebel, O., Schmidt, T., and Kühnel, M.: Ice platelets below Weddell Sea landfast sea ice, Annals of Glaciology, 56, 175-190, 2015.

Hoppmann, M., Richter, M. E., Smith, I. J., Jendersie, S., Langhorne, P. J., Thomas, D. N., and Dieckmann, G. S.: Platelet ice, the Southern Ocean's hidden ice: a review, Annals of Glaciology, 1-28, 2020.

Huguet, C., de Lange, G. J., Gustafsson, Ö., Middelburg, J. J., Damsté, J. S. S., and Schouten, S.: Selective preservation of soil organic matter in oxidized marine sediments (Madeira Abyssal Plain), Geochimica et Cosmochimica Acta, 72, 6061-6068, 2008.

Iacono, M. J., Delamere, J. S., Mlawer, E. J., Shephard, M. W., Clough, S. A., and Collins, W. D.: Radiative forcing by long-lived greenhouse gases: Calculations with the AER radiative transfer models, Journal of Geophysical Research: Atmospheres, 113, https://doi.org/10.1029/2008JD009944, 2008.

Jacobs, S. S., Jenkins, A., Giulivi, C. F., and Dutrieux, P.: Stronger ocean circulation and increased melting under Pine Island Glacier ice shelf, Nature Geoscience, 4, 519-523, 2011.

Jenkins, A., and Jacobs, S.: Circulation and melting beneath George VI ice shelf, Antarctica, Journal of Geophysical Research: Oceans, 113, https://doi.org/10.1029/2007JC004449, 2008.

Johns, L., Wraige, E., Belt, S., Lewis, C., Massé, G., Robert, J.-M., and Rowland, S.: Identification of a C_{25} highly branched isoprenoid (HBI) diene in Antarctic sediments, Antarctic sea-ice diatoms and cultured diatoms, Organic Geochemistry, 30, 1471-1475, 1999.

Kalanetra, K. M., Bano, N., and Hollibaugh, J. T.: Ammonia-oxidizing Archaea in the Arctic Ocean and Antarctic coastal waters, Environmental Microbiology, 11, 2434-2445, 2009.

Khazendar, A., Rignot, E., Schroeder, D.M., Seroussi, H., Schodlok, M.P., Scheuchl, B., Mouginot, J., Sutterley, T.C., Velicogna, I.: Rapid submarine ice melting in the grounding zones of ice shelves in West Antarctica. Nature communications 7, 1-8, 2016.

Kim, J.-H., Van der Meer, J., Schouten, S., Helmke, P., Willmott, V., Sangiorgi, F., Koç, N., Hopmans, E. C., and Damsté, J. S. S.: New indices and calibrations derived from the distribution of crenarchaeal isoprenoid tetraether lipids: Implications for past sea surface temperature reconstructions, Geochimica et Cosmochimica Acta, 74, 4639-4654, 2010.

Kim, J.-H., Crosta, X., Willmott, V., Renssen, H., Bonnin, J., Helmke, P., Schouten, S., and Sinninghe Damsté, J. S.: Holocene subsurface temperature variability in the eastern Antarctic continental margin, Geophysical Research Letters, 39, https://doi.org/10.1029/2012GL051157, 2012.

Klinck, J. M., Hofmann, E. E., Beardsley, R. C., Salihoglu, B., and Howard, S.: Water-mass properties and circulation on the WAP Continental Shelf in Austral Fall and Winter 2001, Deep Sea Research Part II: Topical Studies in Oceanography, 51, 1925-1946, 2004.

Köhler, P., Nehrbass-Ahles, C., Schmitt, J., Stocker, T. F., and Fischer, H.: A 156 kyr smoothed history of the atmospheric greenhouse gases CO_2, CH_4, and N_2O and their radiative forcing, Earth Syst. Sci. Data, 9, 363-387, 2017.

Lamping, N., Müller, J., Esper, O., Hillenbrand, C.-D., Smith, J. A., and Kuhn, G.: Highly branched isoprenoids reveal onset of deglaciation followed by dynamic sea-ice conditions in the western Amundsen Sea, Antarctica, Quaternary Science Reviews, 228, https://doi.org/10.1016/j.quascirev.2019.106103, 2020.

Lange, M., Ackley, S., Wadhams, P., Dieckmann, G., and Eicken, H.: Development of sea ice in the Weddell Sea, Annals of Glaciology, 12, 92-96, 1989.

Langhorne, P., Hughes, K., Gough, A., Smith, I., Williams, M., Robinson, N., Stevens, C., Rack, W., Price, D., and Leonard, G.: Observed platelet ice distributions in Antarctic sea ice: An index for ocean-ice shelf heat flux, Geophysical Research Letters, 42, 5442-5451, 2015.

Leventer, A.: The fate of Antarctic "sea ice diatoms" and their use as paleoenvironmental indicators, Antarctic sea ice. Biological processes, interactions and variability, 121-137, 1998.

Li, X., Holland, D.M., Gerber, E.P. and Yoo, C.:Impacts of the north and tropical Atlantic Ocean on the Antarctic Peninsula and sea ice. Nature 505, 538-542, 2014.

Liu, J., Curry, J. A., and Martinson, D. G.: Interpretation of recent Antarctic sea ice variability, Geophysical Research Letters, 31, https://doi.org/10.1029/2003GL018732, 2004.

Liu, R., Han, Z., Zhao, J., Zhang, H., Li, D., Ren, J., Pan, J., Zhang, H.: Distribution and source of glycerol dialkyl glycerol tetraethers (GDGTs) and the applicability of GDGT-based temperature proxies in surface sediments of Prydz Bay, East Antarctica. Polar Research, 2020.

Locarnini, R. A., Mishonov, A. V., Antonov, J. I., Boyer, T. P., Garcia, H. E., Baranova, O. K., Zweng, M. M., Paver, C. R., Reagan, J. R., and Johnson, D. R.: World ocean atlas 2013. Volume 1, Temperature, NOAA Atlas NESDIS 73, 40 pp., doi: 10.7289/V55X26VD, 2013.

Lohmann, G., Butzin, M., Eissner, N., Shi, X., and Stepanek, C.: Abrupt climate and weather changes across time scales, Paleoceanography and Paleoclimatology, 35, https://doi.org/10.1029/2019PA003782, 2020.

López-García, P., Rodriguez-Valera, F., Pedrós-Alió, C., and Moreira, D.: Unexpected diversity of small eukaryotes in deep-sea Antarctic plankton, Nature, 409, 603-607, 2001.

Lorenz, S. J., and Lohmann, G.: Acceleration technique for Milankovitch type forcing in a coupled atmosphere-ocean circulation model: method and application for the Holocene, Climate Dynamics, 23, 727-743, 2004.

Lott, F.: Alleviation of stationary biases in a GCM through a mountain drag parameterization scheme and a simple representation of mountain lift forces, Monthly weather review, 127, 788-801, 1999.

Loveland, T. R., Reed, B. C., Brown, J. F., Ohlen, D. O., Zhu, Z., Yang, L., and Merchant, J. W.: Development of a global land cover characteristics database and IGBP DISCover from 1 km AVHRR data, Int. J. Remote Sens., 21, 1303-1330, 2000.

Lü, X., Liu, X.-L., Elling, F. J., Yang, H., Xie, S., Song, J., Li, X., Yuan, H., Li, N., and Hinrichs, K.-U.: Hydroxylated isoprenoid GDGTs in Chinese coastal seas and their potential as a paleotemperature proxy for mid-to-low latitude marginal seas, Organic Geochemistry, 89-90, 31-43, 2015.

Massé, G., Belt, S. T., Crosta, X., Schmidt, S., Snape, I., Thomas, D. N., and Rowland, S. J.: Highly branched isoprenoids as proxies for variable sea ice conditions in the Southern Ocean, Antarctic Science, 23, 487-498, 2011.

Massom, R. A., Scambos, T. A., Bennetts, L. G., Reid, P., Squire, V. A., and Stammerjohn, S. E.: Antarctic ice shelf disintegration triggered by sea ice loss and ocean swell, Nature, 558, 383-389, 2018.

Medlin, L.: Berkeleya spp. from Antarctic waters, including Berkeleya adeliensis, sp. nov., a new tube dwelling diatom from the undersurface of sea-ice, Beihefte zur Nova Hedwigia, 100, 77-89, 1990.

Meredith, M. P., Woodworth, P. L., Chereskin, T. K., Marshall, D. P., Allison, L. C., Bigg, G. R., Donohue, K., Heywood, K. J., Hughes, C. W., and Hibbert, A.: Sustained monitoring of the Southern Ocean at Drake Passage: Past achievements and future priorities, Reviews of Geophysics, 49, https://doi.org/10.1029/2010RG000348, 2011.

Meyers, P. A.: Organic geochemical proxies of paleoceanographic, paleolimnologic, and paleoclimatic processes, Organic geochemistry, 27, 213-250, 1997.

Moore, J. K., and Abbott, M. R.: Surface chlorophyll concentrations in relation to the Antarctic Polar Front: seasonal and spatial patterns from satellite observations, Journal of Marine Systems, 37, 69-86, 2002.

Müller, J., Wagner, A., Fahl, K., Stein, R., Prange, M., and Lohmann, G.: Towards quantitative sea ice reconstructions in the northern North Atlantic: A combined biomarker and numerical modelling approach, Earth and Planetary Science Letters, 306, 137-148, 2011.

Müller, J., and Stein, R.: High-resolution record of late glacial and deglacial sea ice changes in Fram Strait corroborates ice–ocean interactions during abrupt climate shifts, Earth and Planetary Science Letters, 403, 446-455, 2014.

975 Nakayama, Y., Schröder, M., Hellmer, H.H.: From circumpolar deep water to the glacial meltwater
976 plume on the eastern Amundsen Shelf. Deep Sea Research Part I: Oceanographic Research
977 Papers 77, 50-62, 2013.
978 Nakayama, Y., Menemenlis, D., Zhang, H., Schodlok, M. and Rignot, E.: Origin of Circumpolar
979 Deep Water intruding onto the Amundsen and Bellingshausen Sea continental shelves. Nature
980 Communications 9, 3403, 2018.
981 Nicholls, K. W., Østerhus, S., Makinson, K., Gammelsrød, T., and Fahrbach, E.: Ice-ocean processes
982 over the continental shelf of the southern Weddell Sea, Antarctica: A review, Reviews of
983 Geophysics, 47, https://doi.org/10.1029/2007RG000250, 2009.
984 Nichols, P. D., Palmisano, A. C., Volkman, J. K., Smith, G. A., and White, D. C.: Occurrence of an
985 isoprenoid C_{25} diunasaturated alkene and high neutral lipid content in Antarctic sea-ice diatom
986 communities 1, Journal of Phycology, 24, 90-96, 1988.
987 Nielsdóttir, M. C., Bibby, T. S., Moore, C. M., Hinz, D. J., Sanders, R., Whitehouse, M., Korb, R.,
988 and Achterberg, E. P.: Seasonal and spatial dynamics of iron availability in the Scotia Sea, Marine
989 Chemistry, 130, 62-72, 2012.
990 Nolting, R., De Baar, H., Van Bennekom, A., and Masson, A.: Cadmium, copper and iron in the
991 Scotia Sea, Weddell Sea and Weddell/Scotia confluence (Antarctica), Marine Chemistry, 35,
992 219-243, 1991.
993 Orsi, A. H., Whitworth III, T., and Nowlin Jr, W. D.: On the meridional extent and fronts of the
994 Antarctic Circumpolar Current, Deep Sea Research Part I: Oceanographic Research Papers, 42,
995 641-673, 1995.
996 Otto-Bliesner, B., Brady, E., Zhao, A., Brierley, C., Axford, Y., Capron, E., Govin, A., Hoffman, J.,
997 Isaacs, E., and Kageyama, M.: Large-scale features of Last Interglacial climate: Results from
998 evaluating the lig127k simulations for CMIP6-PMIP4, Climate of the Past, 17, 63-94, 2021.
999 Otto-Bliesner, B. L., Braconnot, P., Harrison, S. P., Lunt, D. J., Abe-Ouchi, A., Albani, S., Bartlein,
1000 P. J., Capron, E., Carlson, A. E., and Dutton, A.: The PMIP4 contribution to CMIP6–Part 2: Two
1001 interglacials, scientific objective and experimental design for Holocene and Last Interglacial
1002 simulations, Geoscientific Model Development, 10, 3979-4003, 2017.

1003 Park, E., Hefter, J., Fischer, G., Iversen, M. H., Ramondenc, S., Nöthig, E.-M., and Mollenhauer,
1004 G.: Seasonality of archaeal lipid flux and GDGT-based thermometry in sinking particles of high-
1005 latitude oceans: Fram Strait (79° N) and Antarctic Polar Front (50° S), Biogeosciences, 16, 2247-
1006 2268, 2019.
1007 Parkinson, C. L., and Cavalieri, D. J.: Antarctic sea ice variability and trends, 1979-2010, The
1008 Cryosphere, 6, 871-880, 2012.
1009 Parkinson, C. L.: A 40-y record reveals gradual Antarctic sea ice increases followed by decreases at
1010 rates far exceeding the rates seen in the Arctic, Proceedings of the National Academy of Sciences,
1011 116, 14414-14423, 2019.
1012 Paul, S., Willmes, S., and Heinemann, G.: Long-term coastal-polynya dynamics in the southern
1013 Weddell Sea from MODIS thermal-infrared imagery, The Cryosphere, 9, 2027-2041, 2015.
1014 Pritchard, H., Ligtenberg, S., Fricker, H., Vaughan, D., Van den Broeke, M., and Padman, L.:
1015 Antarctic ice-sheet loss driven by basal melting of ice shelves, Nature, 484, 502-505, 2012.
1016 Raddatz, T., Reick, C., Knorr, W., Kattge, J., Roeckner, E., Schnur, R., Schnitzler, K.-G., Wetzel,
1017 P., and Jungclaus, J.: Will the tropical land biosphere dominate the climate–carbon cycle
1018 feedback during the twenty-first century?, Climate dynamics, 29, 565-574, 2007.
1019 Riaux-Gobin, C., and Poulin, M.: Possible symbiosis of Berkeleya adeliensis Medlin, Synedropsis
1020 fragilis (Manguin) Hasle et al. and Nitzschia lecointei Van Heurck (Bacillariophyta) associated
1021 with land-fast ice in Adélie Land, Antarctica, Diatom Research, 19, 265-274, 2004.
1022 Riaux-Gobin, C., Dieckmann, G. S., Poulin, M., Neveux, J., Labrune, C., and Vetion, G.:
1023 Environmental conditions, particle flux and sympagic microalgal succession in spring before the
1024 sea-ice break-up in Adélie Land, East Antarctica, Polar Research, 32,
1025 https://doi.org/10.3402/polar.v32i0.19675, 2013.
1026 Rignot, E., Mouginot, J., Scheuchl, B., Van Den Broeke, M., Van Wessem, M.J., Morlighem, M.:
1027 Four decades of Antarctic Ice Sheet mass balance from 1979–2017. Proceedings of the National
1028 Academy of Sciences 116, 1095-1103, 2019.
1029 Rintoul, S., Hughes, C., and Olbers, D.: The Antarctic circumpolar current system, International
1030 Geophysics, 77, 271-302, 2001.

1031 Roeckner, E., Dümenil, L., Kirk, E., Lunkeit, F., Ponater, M., Rockel, B., Sausen, R., and Schlese,
1032 U.: The Hamburg version of the ECMWF model (ECHAM), Research activities in atmospheric
1033 and oceanic modelling. CAS/JSC Working Group on Numerical Experimentation, 13, 7.1-7.4,
1034 1989.
1035 Rontani, J.-F., Smik, L. and Belt, S.T.: Autoxidation of the sea ice biomarker proxy $IPSO_{25}$ in the
1036 near-surface oxic layers of Arctic and Antarctic sediments, Organic Geochemistry 129, 63-76,
1037 2019.
1038 Rontani, J.-F., Belt, S.T. and Amiraux, R.: Biotic and abiotic degradation of the sea ice diatom
1039 biomarker IP_{25} and selected algal sterols in near-surface Arctic sediments, Organic Geochemistry
1040 118, 73-88, 2018.
1041 Sangrà, P., Gordo, C., Hernández-Arencibia, M., Marrero-Díaz, A., Rodríguez-Santana, A., Stegner,
1042 A., Martínez-Marrero, A., Pelegrí, J. L., and Pichon, T.: The Bransfield current system, Deep Sea
1043 Research Part I: Oceanographic Research Papers, 58, 390-402, 2011.
1044 Scambos, T. A., Bell, R. E., Alley, R. B., Anandakrishnan, S., Bromwich, D., Brunt, K.,
1045 Christianson, K., Creyts, T., Das, S., and DeConto, R.: How much, how fast?: A science review
1046 and outlook for research on the instability of Antarctica's Thwaites Glacier in the 21st century,
1047 Global and Planetary Change, 153, 16-34, 2017.
1048 Schmidt, K., Brown, T. A., Belt, S. T., Ireland, L. C., Taylor, K. W., Thorpe, S. E., Ward, P., and
1049 Atkinson, A.: Do pelagic grazers benefit from sea ice? Insights from the Antarctic sea ice proxy
1050 $IPSO_{25}$, 15, 1987-2006, 2018.
1051 Schmidtko, S., Heywood, K. J., Thompson, A. F., and Aoki, S.: Multidecadal warming of Antarctic
1052 waters, Science, 346, 1227-1231, 2014.
1053 Schofield, O., Brown, M., Kohut, J., Nardelli, S., Saba, G., Waite, N., and Ducklow, H.: Changes in
1054 the upper ocean mixed layer and phytoplankton productivity along the West Antarctic Peninsula,
1055 Philosophical Transactions of the Royal Society A: Mathematical, Physical and Engineering
1056 Sciences, 376, https://doi.org/10.1098/rsta.2017.0173, 2018.

1057 Schouten, S., Hopmans, E. C., Schefuß, E., and Sinninghe Damsté, J. S.: Distributional variations in
1058 marine crenarchaeotal membrane lipids: a new tool for reconstructing ancient sea water
1059 temperatures?, Earth and Planetary Science Letters, 204, 265-274, 2002.
1060 Schouten, S., Hopmans, E. C., and Sinninghe Damsté, J. S.: The organic geochemistry of glycerol
1061 dialkyl glycerol tetraether lipids: A review, Organic Geochemistry, 54, 19-61, 2013.
1062 Schröder, M.: The Expedition PS111 of the Research POLARSTERN to the southern Weddell Sea
1063 in 2018, Berichte zur Polar-und Meeresforschung = Reports on polar and marine research, 718,
1064 2018.
1065 Sidorenko, D., Goessling, H., Koldunov, N., Scholz, P., Danilov, S., Barbi, D., Cabos, W., Gurses,
1066 O., Harig, S., and Hinrichs, C.: Evaluation of FESOM2. 0 coupled to ECHAM6. 3: Preindustrial
1067 and HighResMIP simulations, Journal of Advances in Modeling Earth Systems, 11, 3794-3815,
1068 2019.
1069 Smik, L., Belt, S. T., Lieser, J. L., Armand, L. K., and Leventer, A.: Distributions of highly branched
1070 isoprenoid alkenes and other algal lipids in surface waters from East Antarctica: further insights
1071 for biomarker-based paleo sea-ice reconstruction, Organic Geochemistry, 95, 71-80, 2016.
1072 Smith, J.A., Hillenbrand, C.-D., Kuhn, G., Klages, J.P., Graham, A.G.C., Larter, R.D., Ehrmann,
1073 W., Moreton, S.G., Wiers, S., Frederichs, T.: New constraints on the timing of West Antarctic
1074 Ice Sheet retreat in the eastern Amundsen Sea since the Last Glacial Maximum. Glob. Planet.
1075 Change 112, 224-237, 2014.
1076 Smith, J.A., Hillenbrand, C.-D., Kuhn, G., Larter, R.D., Graham, A.G.C., Ehrmann, W., Moreton,
1077 S.G., Forwick, M.: Deglacial history of the West Antarctic Ice Sheet in the western Amundsen
1078 Sea Embayment, Quaternary Science Reviews 30, 488-505, 2011.
1079 Smith, J.A., Andersen, T., Shortt, M., Gaffney, A., Truffer, M., Stanton, T.P., Bindschadler, R.,
1080 Dutrieux, P., Jenkins, A., Hillenbrand, C.-D.: Sub-ice-shelf sediments record history of twentieth-
1081 century retreat of Pine Island Glacier, Nature 541, 77-80, 2017.
1082 Spencer-Jones, C. L., McClymont, E. L., Bale, N. J., Hopmans, E. C., Schouten, S., Müller, J.,
1083 Abrahamsen, E. P., Allen, C., Bickert, T., Hillenbrand, C. D., Mawbey, E., Peck, V., Svalova,
1084 A., and Smith, J. A.: Archaeal Intact Polar Lipids in Polar Waters: A Comparison Between the

1085 Amundsen and Scotia Seas, Biogeosciences Discuss. [preprint], https://doi.org/10.5194/bg-2020-
1086 333, in review, 2020.
1087 Stevens, B., Giorgetta, M., Esch, M., Mauritsen, T., Crueger, T., Rast, S., Salzmann, M., Schmidt,
1088 H., Bader, J., and Block, K.: Atmospheric component of the MPI-M Earth system model:
1089 ECHAM6, Journal of Advances in Modeling Earth Systems, 5, 146-172, 2013.
1090 Stocker, T. F., Qin, D., Plattner, G.-K., Tignor, M., Allen, S. K., Boschung, J., Nauels, A., Xia, Y.,
1091 Bex, V., and Midgley, P. M.: The physical science basis. Contribution of working group I to the
1092 fifth assessment report of the intergovernmental panel on climate change, Computational
1093 Geometry, 18, 95-123, 2013.
1094 Tesi, T., Belt, S., Gariboldi, K., Muschitiello, F., Smik, L., Finocchiaro, F., Giglio, F., Colizza, E.,
1095 Gazzurra, G., and Giordano, P.: Resolving sea ice dynamics in the north-western Ross Sea during
1096 the last 2.6 ka: From seasonal to millennial timescales, Quaternary Science Reviews, 237,
1097 http://dx.doi.org/10.1016/j.quascirev.2020.106299, 2020.
1098 Thomas, D. N.: Sea ice, John Wiley & Sons, 2017.
1099 Thompson, A. F., Heywood, K. J., Thorpe, S. E., Renner, A. H., and Trasviña, A.: Surface circulation
1100 at the tip of the Antarctic Peninsula from drifters, Journal of Physical Oceanography, 39, 3-26,
1101 2009.
1102 Thompson, A. F., Stewart, A. L., Spence, P., and Heywood, K. J.: The Antarctic Slope Current in a
1103 changing climate, Reviews of Geophysics, 56, 741-770, 2018.
1104 Turner, J., Orr, A., Gudmundsson, G. H., Jenkins, A., Bingham, R. G., Hillenbrand, C.-D., and
1105 Bracegirdle, T. J.: Atmosphere-ocean-ice interactions in the Amundsen Sea Embayment, West
1106 Antarctica, Reviews of Geophysics, 55, 235-276, 2017.
1107 Turner, J., Guarino, M.V., Arnatt, J., Jena, B., Marshall, G.J., Phillips, T., Bajish, C.C., Clem, K.,
1108 Wang, Z., Andersson, T., Murphy, E.J., Cavanagh, R.: Recent Decrease of Summer Sea Ice in
1109 the Weddell Sea, Antarctica, Geophysical Research Letters 47, e2020GL087127, 2020.
1110 Valcke, S.: The OASIS3 coupler: A European climate modelling community software, Geoscientific
1111 Model Development, 6, 373-388, 2013.

1112 Vaughan, D. G., Marshall, G. J., Connolley, W. M., Parkinson, C., Mulvaney, R., Hodgson, D. A.,
1113 King, J. C., Pudsey, C. J., and Turner, J.: Recent rapid regional climate warming on the Antarctic
1114 Peninsula, Climatic change, 60, 243-274, 2003.
1115 Vaughan, D. G.: West Antarctic Ice Sheet collapse–the fall and rise of a paradigm, Climatic Change,
1116 91, 65-79, 2008.
1117 Vernet, M., Geibert, W., Hoppema, M., Brown, P. J., Haas, C., Hellmer, H., Jokat, W., Jullion, L.,
1118 Mazloff, M., and Bakker, D.: The Weddell Gyre, Southern Ocean: present knowledge and future
1119 challenges, Reviews of Geophysics, 57, 623-708, 2019.
1120 Volkman, J. K.: Lipid markers for marine organic matter, in: Marine organic matter: Biomarkers,
1121 isotopes and DNA, Springer, 27-70, 2006.
1122 Vorrath, M.-E., Müller, J., Esper, O., Mollenhauer, G., Haas, C., Schefuß, E., and Fahl, K.: Highly
1123 branched isoprenoids for Southern Ocean sea ice reconstructions: a pilot study from the WAP,
1124 Biogeosciences, 16, 2961-2981, 2019.
1125 Vorrath, M.-E., Müller, J., Rebolledo, L., Cárdenas, P., Shi, X., Esper, O., Opel, T., Geibert, W.,
1126 Muñoz, P., and Haas, C.: Sea ice dynamics in the Bransfield Strait, Antarctic Peninsula, during
1127 the past 240 years: a multi-proxy intercomparison study, Climate of the Past, 16, 2459-2483,
1128 2020.
1129 Wang, Z., Turner, J., Wu, Y., Liu, C.: Rapid Decline of Total Antarctic Sea Ice Extent during 2014–
1130 16 Controlled by Wind-Driven Sea Ice Drift. Journal of Climate 32, 5381-5395, 2019.
1131 Witus, A.E., Branecky, C.M., Anderson, J.B., Szczuciński, W., Schroeder, D.M., Blankenship, D.D.,
1132 Jakobsson, M.: Meltwater intensive glacial retreat in polar environments and investigation of
1133 associated sediments: example from Pine Island Bay, West Antarctica, Quaternary Science
1134 Reviews, 85, 99–118, 2014.
1135 Xiao, X., Fahl, K., Müller, J., and Stein, R.: Sea-ice distribution in the modern Arctic Ocean:
1136 Biomarker records from trans-Arctic Ocean surface sediments, Geochimica et Cosmochimica
1137 Acta, 155, 16-29, 2015.

Zamelczyk, K., Rasmussen, T. L., Husum, K., Haflidason, H., de Vernal, A., Ravna, E. K., Hald, M., and Hillaire-Marcel, C.: Paleoceanographic changes and calcium carbonate dissolution in the central Fram Strait during the last 20 ka, Quaternary Research, 78, 405-416, 2012.

Zielinski, U., Gersonde, R., Sieger, R., and Fütterer, D.: Quaternary surface water temperature estimations: Calibration of a diatom transfer function for the Southern Ocean, Paleoceanography and Paleoclimatology, 13, 365-383, 1998.

Zwally, H. J.: Antarctic sea ice, 1973-1976: Satellite passive-microwave observations, Scientific and Technical Information Branch, National Aeronautics and Space, 1983.